Stability Analysis and Control Design of Grid-Forming Converters With DC-Link Effect

Chenhang Xu, *Student Member, IEEE*, Zhixiang Zou, *Senior Member, IEEE*, Xinlei Liu, *Student Member, IEEE*, Meng Huang, *Member, IEEE*, Wu Chen, *Senior Member, IEEE*, and Zheng Wang, *Senior Member, IEEE*

***Abstract*—Grid-forming converters are increasingly utilized as the interface between distributed energy resources and utilities, owing to their advantageous features. However, they may encounter transient stability issues during grid faults, particularly when considering the dc-link effect. This article establishes a transient energy function which enables stability analysis of the grid-forming converter with dc-link effect based on Lyapunov direct method, revealing that transient instability is mainly induced by power imbalance and negative damping effect. To address this issue, an enhanced dc-link voltage control is proposed to facilitate temporarily energy storage and inertia adjustment, thereby improving transient stability and avoiding possible overvoltage in grid-forming converters. Theoretical analysis and validations have been provided to verify the effectiveness.**

***Index Terms*—DC-link voltage control (DVC), grid-forming (GFM) converters, Lyapunov energy function, transient stability.**

I. Introduction

In recent years, the integration of distributed energy sources into the power grid has significantly increased. Distributed energy sources are commonly integrated to the power grid through power electronic based converters to realize energy conversion [1]. These converters, however, generally have limited thermal capacity and significantly less inertia compared to traditional synchronous generators (SGs). The reduced inertia diminishes their capability to withstand network disturbances, introducing substantial challenges to the stability and secure operation of power systems, especially in circumstances with high penetration of power electronic interfaces [2]. To mitigate these issues, grid-forming (GFM) converters which are able to form voltage and support frequency [3], [4], [5], [6], [7], [8] have been developed. Among the various grid-forming strategies, virtual synchronous generator (VSG) has emerged as a prominent solution, effectively replicating the inertial and damping characteristics of conventional SGs by emulating their dynamics to enhance system resilience against disturbances [9], [10], [11], [12].

The studies of the transient stability of GFM converters have drawn wide attention. Phase portrait and equal area criterion (EAC) are used in [13] and [14], highlight that there are two primary factors that can lead to loss of synchronization (LOS): the lack of equilibrium points and insufficient damping. In these studies, an ideal dc voltage source is assumed. However, different from SGs, VSGs are incapable of absorbing/ delivering any kinetic energy and thus an energy storage system and dc-link capacitor is usually needed in the dc side [5], [15], [16], [17]. To achieve instantaneous power balance between dc side and ac side of the GFM converters, dc-link voltage control (DVC) is adopted [18]. In recent literature considering dc-link voltage dynamics, V-square control, which uses stored energy and the square of dc-link voltage as feedback signals to change active power reference of GFM converters, are adopted to avoid the dependence of the closed-loop dynamics of DVC on its steady-state operating point [19], [20]. The introduction of dc-link effect will give rise to more transient stability issues. Phase portrait is drawn in [21] and [22], pointing out that DVC would jeopardize the transient stability of both grid-following converter and GFM converter, even with a nonsevere grid voltage dip. Subsequently, the parametric effect of DVC on transient stability is performed in 3-D phase space since the phase portrait cannot fully reveal the parametric effect of high-order model [23]. Bifurcation theory is used in [24], finding that dc-link voltage dynamic can introduce unstable limit cycles, which may lead to LOS. In [25], transient stability of the droop controlled GFM converter with dc-link effect is investigated based on Lyapunov function and optimization method, finding that the dc-link voltage dynamic can result in the shrinkage of attraction region. However, above-mentioned transient stability analysis methods rely on numerical calculation and optimization, thus provide little physical insight. In addition to the numerical analysis methods, EAC is employed in [26] and [27] to identify the impact of dc-link voltage dynamics on the accelerating and decelerating area of VSG, which reveals its deteriorative effect on transient stability. However, the EAC is not suitable for system containing negative damping, which equivalently increases the accelerating area in EAC. The fourth-order nonlinear system is decomposed by a slow system and a fast system, thus simplifies the analysis

Received 5 October 2024; revised 18 December 2024; accepted 16 January 2025. Date of publication 27 January 2025; date of current version 26 February 2025. This work was supported in part by the National Natural Science Foundation of China under Grant 52377171, and in part by the Fundamental Research Funds for the Central Universities under Grant 2242024K40030. Recommended for publication by Associate Editor Alon Kuperman. *(Corresponding author: Zhixiang Zou.)*

Chenhang Xu, Zhixiang Zou, Xinlei Liu, Wu Chen, and Zheng Wang are with the School of Electrical Engineering, Southeast University, Nanjing 210096, China (e-mail: xuch@seu.edu.cn; zzou@seu.edu.cn; liuxinlei@seu.edu.cn; chenwu@seu.edu.cn; zwang@seu.edu.cn).

Meng Huang is with the Hubei Key Laboratory of Power Equipment and System Security for Integrated Energy and School of Electrical Engineering and Automation, Wuhan University, Wuhan 410000, China (e-mail: meng.huang@whu.edu.cn).

Color versions of one or more figures in this article are available at https://doi.org/10.1109/TPEL.2025.3534470.

Digital Object Identifier 10.1109/TPEL.2025.3534470

of DVC control parameters design guidelines [28]. However, such singular perturbation-based analysis method is only suitable for systems where the control blocks exhibit significantly different bandwidths. Overall, the analytical method designed for high-order nonlinear system that can offer clear physical insight, facilitate stability assessment and provide parameter guidelines is still worth studying.

To mitigate the transient stability issues introduced by DVC, several stabilizing control methods have been proposed in previous research works. The current saturation limiter is cancelled when the dc-link voltage is increasing to accelerate the converging process in [29] to tackle its adverse impact on dc-link voltage. In [30], two additional control loops are integrated into electric synchronous machine: the error dc-link voltage is feedforwarded to the phase angle to increase the damping torque and to the amplitude of output voltage to further improve the energy dissipation of the system. An adaptive-output-voltage-regulation-based solution is proposed in [31] to avoid possible undervoltage. The main idea is to feedforward the error of dc-link voltage to the output voltage and downscale the feedback power to accelerate the converging process. Above-mentioned control methods focuses on the dc-link overvoltage or undervoltage issues rather than transient synchronous stability. A paralleled connection of the DVC and power synchronization loop is employed in [22], which leads to an additional control degree-of-freedom for flexible damping design. Currently, research on stability enhancement control mainly focus on the ac side of converters, whereas control strategies for the dc side have received limited attention. This imbalanced research emphasis has left the critical issue of transient unbalanced power storage overlooked. More importantly, there is a notable absence of comprehensive control methods that simultaneously alleviate both the risk of LOS and dc-link overvoltage. This article aims to propose a transient stability enhancement control by managing the dc-link capacitor to store the unbalanced power in order to alleviate the energy imbalance and subsequent LOS during transient, while adjusting the inertia to accelerate the converging process during fault in order to alleviate the boost of dc-link voltage. The main contribution of this article can be concluded as follows.

1) A Lyapunov-based energy function of GFM converters with DVC is established, which facilitates the transient stability analysis of GFM converters with fully consideration of dc-link voltage dynamic.
2) The impact of introducing DVC and parametric effect of VSG and DVC on transient stability is analyzed based on the proposed energy function, and the existence of negative damping effect is revealed in the fourth-order system.
3) An enhanced DVC is proposed for GFM converters, which allows the dc-link capacitor to temporarily store the unbalanced power between dc side and ac side of the converter, thus alleviate the risk of LOS caused by power imbalance, and alleviate the risk of overvoltage by adjusting inertia during transient. Its effectiveness under the scenario when current limiter is triggered is also validated.

The rest of this article is organized as follows. In Section II, the large-signal model of the GFM converter considering dc-link effect is established, with its accuracy validated by comparison study. Based on the reduced-order large-signal model, a transient energy function designed for the fourth-order system is proposed. In Section III, the impact of introducing DVC and its parametric effect on the transient stability is analyzed based on Lyapunov direct method and invariance principle. In Section IV, the implementation methods and principles of the proposed control are introduced, with its cost-effective characteristic analyzed. Its effectiveness when converter is overcurrent is subsequently studied. Lastly, the effectiveness of eDVC is confirmed by experimental results in Section V. Finally, Section VI concludes this article.

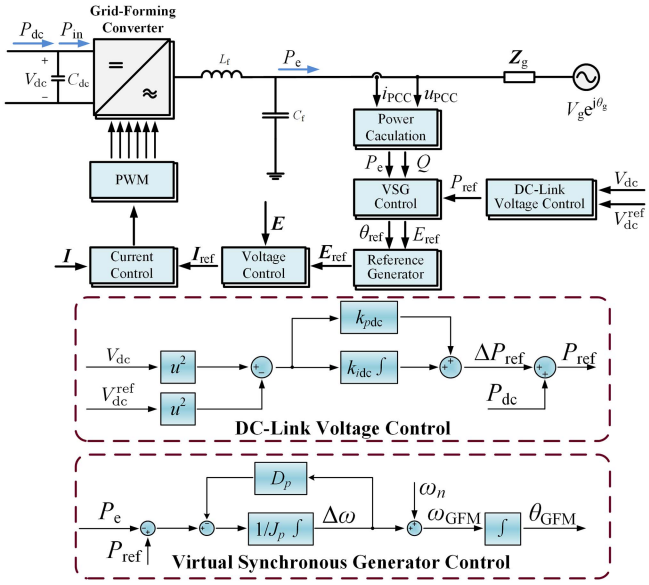

Fig. 1. System configuration and control diagram of the GFM converter [9].

TABLE I
NOMINAL VALUES OF THE STUDIED SYSTEM

Symbol	Description	Nominal Value
P_n	rated active power	10 kW
$V_{\rm dc}^{\rm ref}$	dc-link voltage reference	1000 V
$V_{\rm ac}$	ac voltage (rms)	220 V
$L_{\rm g}$	line impedance	20 mH
J_p, D_p	VSG control parameters	80, 800
$k_{p{\rm dc}}, k_{i{\rm dc}}$	DVC control parameters	0.013, 0.01
$C_{\rm dc}$	dc-link capacitor	4400 μF

II. ENERGY FUNCTION MODELING

Fig. 1 depicts the system configuration and control diagram of GFM converters employing DVC. The ac grid is represented by the voltage source $V_{\rm g}{\rm e}^{{\rm j}\theta_{\rm g}}$ and the grid impedance $\mathbf{Z}_{\rm g}$. $V_{\rm dc}$ and $V_{\rm dc}^{\rm ref}$ represent the dc-link voltage and its reference, respectively. The circuit parameters of the studied system are summarized in Table I.

VSG control is employed as a representative power synchronization loop of the GFM control in this article. The active power control loop of the VSG imitates the rotor motion characteristics of the SG and provides phase reference $\theta_{\rm GFM}$, while the $Q-V$

droop control is implemented in the reactive power control loop to regulate the output voltage amplitude of GFM converter, whose expression are as follows:

$$\theta_{\mathrm{GFM}} = \frac{1}{J_p}\int\left(\int\left(P_{\mathrm{ref}} - P_{\mathrm{e}} - D_p\Delta\omega\right) + \omega_n\right) \tag{1}$$

$$E_{\mathrm{ref}} = E_n + K_Q\left(Q_{\mathrm{ref}} - Q_{\mathrm{e}}\right) \tag{2}$$

where J_p and D_p represent the virtual inertia and virtual damping of the VSG. The K_Q is the droop coefficient of the reactive power control loop. P_{ref} and Q_{ref} are the active power reference and reactive power reference of the GFM converter, respectively.

The phase and voltage amplitude references are combined to generate the voltage reference vector $\boldsymbol{E}_{\mathrm{ref}}$. The inner voltage loop regulates the output voltage $\boldsymbol{E}$ to track the reference. A current loop is cascaded to the voltage loop to actively damp the LC resonance and thus enhance the system stability [13]. In practice, the bandwidth of the inner voltage and current control loop are designed to be much higher than that of VSG and DVC. Hence, the dual loop voltage control can be simplified as a unity gain with ideal reference tracking in the transient stability analysis [31], i.e., $\boldsymbol{E} = \boldsymbol{E}_{\mathrm{ref}}$.

The active power reference of the GFM converter is generated by DVC, which is

$$P_{\mathrm{ref}} = \left(k_{p\mathrm{dc}} + k_{i\mathrm{dc}}\int\right)\cdot\left(\left(V_{\mathrm{dc}}\right)^2 - \left(V_{\mathrm{dc}}^{\mathrm{ref}}\right)^2\right) \tag{3}$$

where $k_{p\mathrm{dc}}$ and $k_{i\mathrm{dc}}$ represent the proportional gain and integral gain of the PI controller in DVC.

The power angle is defined as $\delta = \theta_{\mathrm{GFM}} - \theta_{\mathrm{g}}$. P_{e} and Q denote the output active and reactive power of converter, whose expressions are

$$P_{\mathrm{e}} = \frac{3}{2}EV_{\mathrm{g}}B_{\mathrm{g}}\sin\delta \tag{4}$$

$$Q = \frac{3}{2}EB_{\mathrm{g}}\left(E - V_{\mathrm{g}}\cos\delta\right) \tag{5}$$

where B_{g} represents the grid susceptance.

Imbalances between the input power on the dc side and the output power on the ac side can lead to variations in the voltage of the dc-link capacitor, which can be derived as

$$P_{\mathrm{dc}} = P_{\mathrm{e}} + \frac{C_{\mathrm{dc}}}{2}\dot{\left(V_{\mathrm{dc}}\right)^2} \tag{6}$$

where C_{dc} represents the dc-link capacitor.

In the light of (1), (3), and (6), according to Fig. 2, the large-signal model of the GFM converter is derived as

$$\begin{cases} \dot{\left(V_{\mathrm{dc}}\right)^2} = \frac{2}{C_{\mathrm{dc}}}\left(P_{\mathrm{dc}} - P_{\mathrm{e}}\right) \\ \dot{P}_{\mathrm{ref}} = k_{i\mathrm{dc}}\cdot\left(\left(V_{\mathrm{dc}}\right)^2 - \left(V_{\mathrm{dc}}^{\mathrm{ref}}\right)^2\right) + \frac{2k_{p\mathrm{dc}}}{C_{\mathrm{dc}}}\cdot\left(P_{\mathrm{dc}} - P_{\mathrm{e}}\right) \\ J_p\cdot\ddot{\delta} = \left(P_{\mathrm{ref}} - P_{\mathrm{e}}\right) - D_p\cdot\dot{\delta}. \end{cases} \tag{7}$$

In order to validate the accuracy of the proposed large-signal model, the full-order circuit simulation for Fig. 1 is conducted, and a comparison verification between full-order model and the large-signal model is proposed. As Fig. 3 shows, the transient response of the large-signal model can well match with the full-order model, thus validating the accuracy of proposed large-signal model.

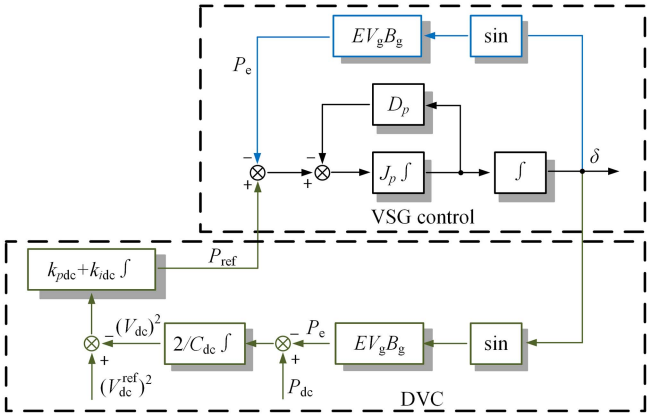

Fig. 2. Large-signal model of the GFM converter considering DC-link effect.

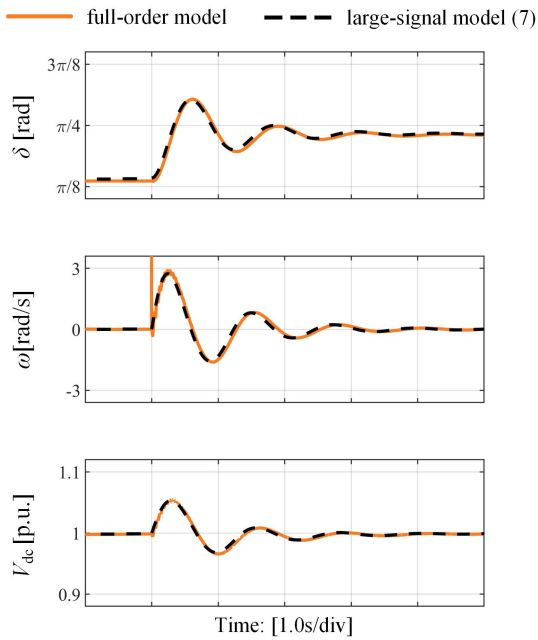

Fig. 3. Comparison of transient response of full-order model and large-signal model (7) under a 0.3 p.u. fault.

The energy function of the GFM converter is derived as follows, with more detailed derivation given in the appendix:

$$\begin{aligned} \mathbf{V}(\omega,\delta,V_{\mathrm{dc}}) = {} & \frac{1}{2}J_p\Delta\omega^2 - P_{\mathrm{dc}}\delta - EV_{\mathrm{g}}B_{\mathrm{g}}\cos\delta \\ & + \xi\cdot\left(\left(V_{\mathrm{dc}}\right)^2 - \left(V_{\mathrm{dc}}^{\mathrm{ref}}\right)^2\right)\cdot\left(-\delta + \delta_{\mathrm{e}}^{\mathrm{s}}\right) \\ & + \xi\cdot\left(\left(V_{\mathrm{dc}}\right)^2 - \left(V_{\mathrm{dc}}^{\mathrm{sat}}\right)^2\right)\cdot\zeta\sin\left(\frac{\pi}{2}\frac{\delta - \delta_{\mathrm{e}}^{\mathrm{s}}}{\delta_{\mathrm{e}}^{\mathrm{u}} - \delta_{\mathrm{e}}^{\mathrm{s}}}\right) \\ & + \frac{k_{i\mathrm{dc}}}{k_{p\mathrm{dc}}}\left(J_p\Delta\omega\delta + \frac{D_p}{2}\left(\delta - \delta_{\mathrm{e}}^{\mathrm{s}}\right)^2\right) + \alpha \end{aligned} \tag{8}$$

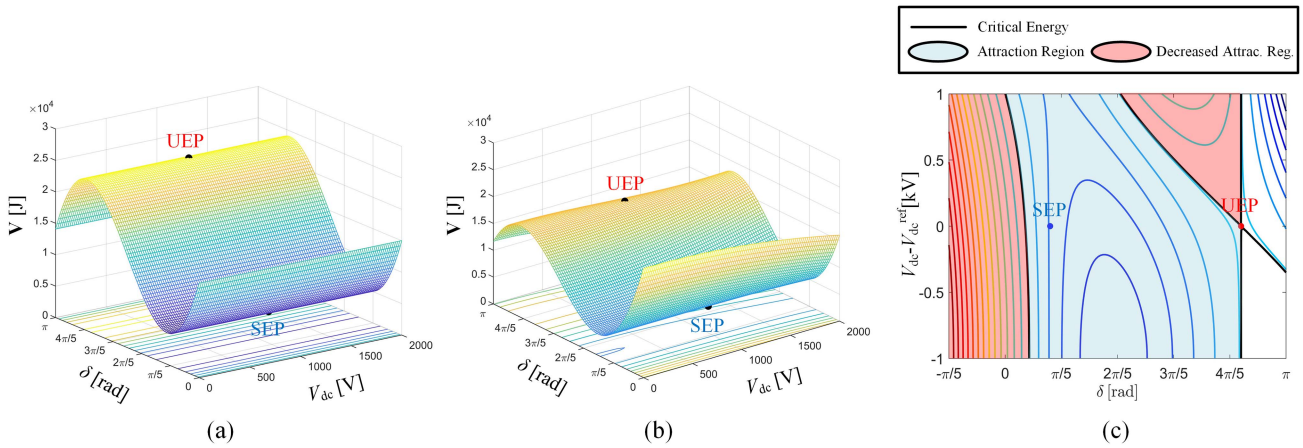

Fig. 4. Transient energy distribution of GFM converter. (a) Neglect DVC. (b) Consider DVC. (c) Change of attraction region.

where $\xi = (k_{\mathrm{pdc}} - \frac{k_{i\mathrm{dc}}}{k_{\mathrm{pdc}}}\frac{C_{\mathrm{dc}}}{4})$. The coefficient ζ is used to regulate the weight of dc-link overvoltage protection term. α is an arbitrary constant to ensure the positive definiteness of the energy function. $\delta_{\mathrm{e}}^{\mathrm{s}}$ and $\delta_{\mathrm{e}}^{\mathrm{u}}$ represent the stable equilibrium point (SEP) and unstable equilibrium point (UEP) of the power angle, which can be calculated as

$$\begin{cases} \delta_{\mathrm{e}}^{\mathrm{s}} = \arcsin\left(P_{\mathrm{dc}}/EV_{\mathrm{g}}B_{\mathrm{g}}\right) \\ \delta_{\mathrm{e}}^{\mathrm{u}} = \pi - \delta_{\mathrm{e}}^{\mathrm{s}}. \end{cases} \tag{9}$$

In the transient energy function (8), $J_p\Delta\omega^2/2$ represents the kinetic energy. $P_{\mathrm{dc}}\delta$ represents the potential energy relative to dc side input power. $EV_{\mathrm{g}}B_{\mathrm{g}}\cos\delta$ represents the electric energy of line impedance. The fourth term of the energy function evaluates the redundant energy from dc side to ac side of the converter, the fifth term represents the stability margin from overvoltage and the sixth term represents the cumulative imbalance energy over time introduced by the integral coefficient of the DVC.

III. Transient Stability Analysis

The Lyapunov direct method [32] is employed to investigate the impact of DVC on the transient stability of the GFM converter, by analyzing its influence on the potential energy distribution. Furthermore, LaSalle's invariance principle and the extended invariance principle [33], [34], [35] are introduced to analyze the parametric effect on the transient stability. Suppose $x \in \mathbb{R}^n$ is the system state for system $\mathrm{d}x/\mathrm{d}t = f(x)$. Let $\boldsymbol{W}(x) : \mathbb{R}^n \to \mathbb{R}$ be C^1 function. l and L are constant. Define bounded region $\Omega_L = \{\boldsymbol{W}(x) \le L < \infty\}$ and bounded region $\bar{\Omega}_l = \{\boldsymbol{W}(x) \le l < L\}$. Suppose $\mathrm{d}\boldsymbol{W}(x)/\mathrm{d}t > 0$ exists in $x \in \bar{\Omega}_l$ and $\mathrm{d}\boldsymbol{W}(x)/\mathrm{d}t \le 0$ for every $x \in| \bar{\Omega}_l$ in Ω_L. Define set $R(x) \in \Omega_L$ satisfies $\mathrm{d}\boldsymbol{W}(x)/\mathrm{d}t = 0$, and set $\bar{\Omega}_l$ is appended. The extended invariance principle is presented as follows:

$$\begin{cases} \bar{\Omega}_l(x) = \{x \in \mathbb{R}^n \mid \boldsymbol{W}(x) \le l < L\} \\ \Omega_L(x) = \left\{x \in \mathbb{R}^n \mid \boldsymbol{W}(x) \le L, \dot{\boldsymbol{W}}(x)_{l<\boldsymbol{W}(x)<L} \le 0\right\} \\ R(x) = \left\{x \in \Omega_L \mid \dot{\boldsymbol{W}}(x) = 0\right\} \cup \bar{\Omega}_l. \end{cases} \tag{10}$$

Every state x^0 starting in stability domain Ω_L converges to $R(x)$ as $t \to \infty$.

A. Impact of Dc-Link Voltage Dynamic

The transient energy of GFM converter with or without considering dc-link effect in $\delta - V_{\mathrm{dc}}$ plane is shown in Fig. 4. The value of transient energy at UEP is defined as critical energy [36], once the transient energy surpasses the critical energy, it implies that the system will exceed UEP, leading to transient instability. The introduction of DVC reduces the critical energy while elevating the transient energy before the SEP, thus decreases the attraction region of the system, as shown in Fig. 4(c), where the red area represents the reduced attraction region of the GFM converter caused by the introduction of DVC.

The detrimental effect of DVC on the stability can be further explained from the perspective of EAC. Ignoring the overvoltage protection term, the $P - \delta$ figure of the GFM converter can be obtained by taking the partial derivative with respect to the power angle of potential energy terms. The equivalent magnetic power P_{m} and the electric power P_{e} are as follows:

$$\begin{cases} P_{\mathrm{m}} = P_{\mathrm{dc}} + \xi \cdot \left((V_{\mathrm{dc}})^2 - \left(V_{\mathrm{dc}}^{\mathrm{ref}}\right)^2\right) + \frac{k_{i\mathrm{dc}}}{k_{p\mathrm{dc}}} D_p \left(\delta - \delta_{\mathrm{e}}^{\mathrm{s}}\right) \\ P_{\mathrm{e}} = EV_{\mathrm{g}}B_{\mathrm{g}}\sin\delta. \end{cases} \tag{11}$$

The integral of the difference between P_{m} and P_{e} with respect to δ, as the sum of the accelerating and decelerating areas in the $P - \delta$ figure, quantifies the change in the kinetic energy during the transient process. When DVC is not considered, P_{m} will always equal to P_{dc} during transient, as P'_{m} shown in Fig. 5(a). When considering the effect of DVC, P_{m} exceeds P_{dc} during fault to release the excessive power in dc-link capacitor, as P_{m} shown in Fig. 5(b), resulting in the increase of accelerating area from S_1 to $S_1 + S_2$ and decrease of decelerating area from $S_3 + S_4$ to S_3, thus exacerbating the overshoot of the power angle. In this regard, the effect of the DVC could compromise the transient stability of the GFM converter. Furthermore, the excess active power P_{dc} will rush into the dc-link capacitor during the converging process of power angle, causing the boost of dc-link

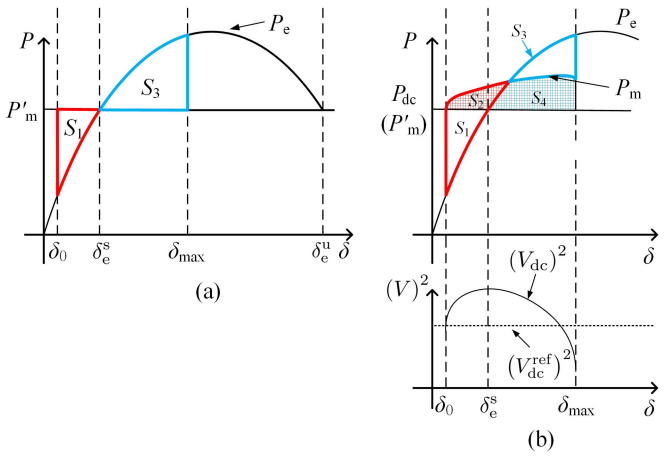

Fig. 5. $P-\delta$ diagram of GFM converter. (a) Neglect DVC. (b) Consider DVC.

voltage, which may trigger the overvoltage protection or even trip the converter.

B. Impact of Control Parameters

1) Impact of VSG Control Parameters: The virtual inertia J_p increases from 1 p.u. to 2 p.u. to identify its effect on the attraction region, and its result is shown in Fig. 6(b). It is observed that the attraction region decreases with the increase of the inertia, which reveals the GFM converter with higher inertia is more prone to lose transient stability. This is due to the fact that, as inertia increases, the system's kinetic energy at the same angular velocity becomes larger, making it easier to surpass critical energy. Meanwhile, larger virtual inertia means slower dynamic of the power angle and longer converging process. This trend leads to a higher boost of dc-link voltage and in turn results in a severer increase of the magnetic power, thus deteriorate the transient stability and heighten the risk of overvoltage.

The virtual damping D_p decreases from 1 p.u. to 0.6 p.u. to identify its effect on the transient stability, and its result is shown in Fig. 6(c). It can be found that the negative damping region, i.e., where $\dot{\mathbf{V}} > 0$ and system energy accumulates rather than dissipates, exceeds the critical energy boundary with insufficient virtual damping. This indicates the system lacks the attraction region according to invariance principle. Consequently, it can be concluded that smaller virtual inertia and larger virtual damping can lead to better stability metrics of the converter. This trend is also applicable when converter undergoes sudden change in active power reference (such as presynchronization process in islanded system) [37], [38].

2) Impact of DVC Parameters: The DVC proportional coefficient $k_{p\mathrm{dc}}$ rises from 1 p.u. to 4 p.u. to identify its effect on the attraction region, and the result is shown in Fig. 6(d). Similarly, the integral coefficient $k_{i\mathrm{dc}}$ is raised from 1 p.u. to 4 p.u., and the corresponding change of attraction region and negative damping area are illustrated in Fig. 6(e). It is observed that the attraction region in $V-\delta$ plane decreases with the increase of $k_{p\mathrm{dc}}$ and the negative damping region in $\omega-\delta$ plane expands with the increase of $k_{p\mathrm{dc}}$ and $k_{i\mathrm{dc}}$. When the extent of dc-link elevation is same, higher DVC parameters will cause more redundant energy to be released from the dc side to the ac side, thereby elevating the transient energy and reducing the attraction region. From the perspective of EAC, higher DVC parameters lead to larger magnetic power during transient to help facilitate faster recovery of the dc-link voltage to its reference, but also cause the increase of accelerating area and decrease of decelerating area. Therefore, the faster dc-link voltage dynamic of GFM converter can adversely affect the transient stability.

3) Impact of Dc-Link Capacitor: The dc-link capacitor C_{dc} is reduced from 1 p.u. to 0.1 p.u. to reveal its effect on stability, with its impact on attraction region shown in Fig. 6(f). It is observed that the negative damping region increases with the decrease of the dc-link capacitor. The smaller the dc-link capacitor, the less unbalanced energy can be stored at the dc side for the same voltage rise according to (6), resulting in larger system redundant energy. Therefore, the GFM converter with larger dc-link capacitor will achieve better transient stability.

C. Comparison With Existing Analysis Methods

To analyze the transient stability of the GFM converters, several stability analysis methods have been proposed in the literature [21], [22], [24], [25], [26]. The advantages and limitations of these stability analysis methods are summarized in Table II.

Compared to the above-mentioned analysis methods, the proposed energy function-based method has insightful physical intuition of instability. The manually constructed energy function facilitates the guidance of control parameters design and fully considers the negative damping effect, thus providing accurate stability assessment. The major limitation is sometimes it is hard to construct the suitable energy function.

IV. Transient Stability Enhancement

As discussed in the previous section, lower potential energy before SEP and higher potential energy at UEP will lead to a larger attraction region, which results in a smaller accelerating area and larger decelerating area, thus reducing the risk of instability. This can be achieved by elevating the dc-link voltage reference according to (8). The adjustment of dc-link voltage reference will cause it to be higher than its actual value, therefore, the magnetic power can be reduced so that it is possible to optimize both the accelerating and decelerating areas.

A. Enhanced DVC

With above-mentioned consideration, a feedback loop from angular speed, namely, the derivative of the power angle, to the dc-link voltage reference is introduced in Fig. 7 to adjust the voltage reference during the accelerating process of the power angle. As shown in Fig. 8(b), by implementing the proposed control loop (I), the reference voltage of the dc-link capacitor is raised at fault instant, as $V_{\mathrm{dc}}^{\mathrm{ref}*}$ in Fig. 8(b). The difference between $(V_{\mathrm{dc}}^{\mathrm{ref}*})^2$ and $(V_{\mathrm{dc}})^2$ will adjust P_{m} to be even lower than P_{dc}, as P_{m}^* in Fig. 8(b), allowing the excessive active power to be temporarily stored in the dc-link capacitor. This results in

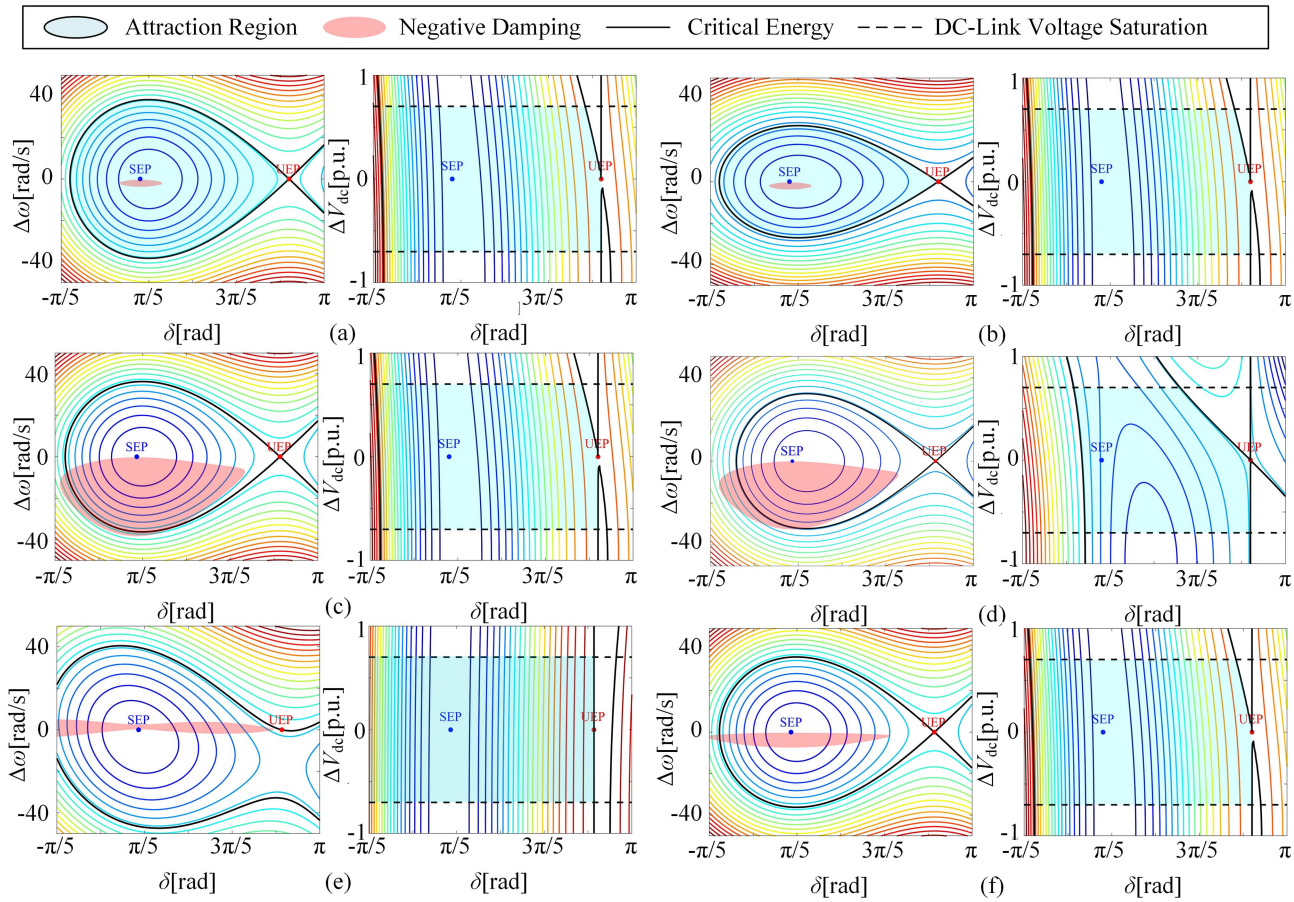

Fig. 6. Estimated attraction domain of GFM converter. (a) Nominal control parameters. (b) Increase virtual inertia. (c) Decrease virtual damping. (d) Increase proportional gain in DVC. (e) Increase integral gain in DVC. (f) Decrease DC-link capacitor.

TABLE II
COMPARISON OF PROPOSED LYAPUNOV FUNCTION-BASED ANALYSIS AND EXISTING STABILITY ANALYSIS METHODS

Stability analysis methods	Advantages	Limitations
Phase portrait [21], [22]	· applied for higher-order nonlinear system	· no physical insight · cannot present dc-link dynamic
Bifurcation-based analysis [24]	· applied for higher-order nonlinear system · guide for control parameters design	· less physical insight · computational burden
Optimization and Lyapunov function-based analysis [25]	· applied for higher-order nonlinear system · easy to establish energy function	· less physical insight · computational burden
EAC [26]	· insightful physical intuition	· neglect negative damping · cannot used for stability assessment
Proposed Lyapunov function	**· insightful physical intuition · guide for control parameters design · consider negative damping**	**· hard to establish energy function**

the decrease of accelerating area from $S_1 + S_2$ to S_1 and the increase of decelerating area from $S_3 - S_4$ to S_3, thereby alleviating the risk of transient instability. The overvoltage caused by continuous mismatch of ac side output power and dc side input power of the GFM converter can also be avoided.

Under the circumstance that equilibrium point exists, a larger virtual inertia increases the overshoot of the power angle, which makes it easier to cross UEP. Therefore, a smaller inertia during transient helps to maintain the synchronization of the GFM converter [39]. Meanwhile, a faster converging process of the power angle results in a smaller boost of dc-link voltage [31]. Furthermore, since the GFM converter is not able to provide sufficient inertia after reaching its current limit or losing synchronization, maintaining its stability and preventing it from tripping should be the priority during large disturbance [12]. Therefore, the converging dynamic should be fastened during transient for the concern of both transient stability and dc-link overvoltage. To achieve this target, a feedback loop between the $\ddot{\delta}$ and the dc-link voltage reference is introduced in Fig. 7. As swing equation (12) shows, the proposed control loop (II) adjusts the inertia equivalently, thus accelerating the converging dynamic of the GFM converter. Consequently, the overshoot of

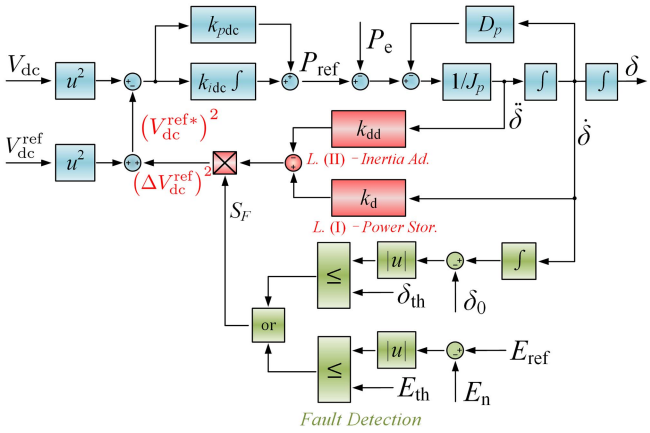

Fig. 7. Control diagram of the enhanced DVC.

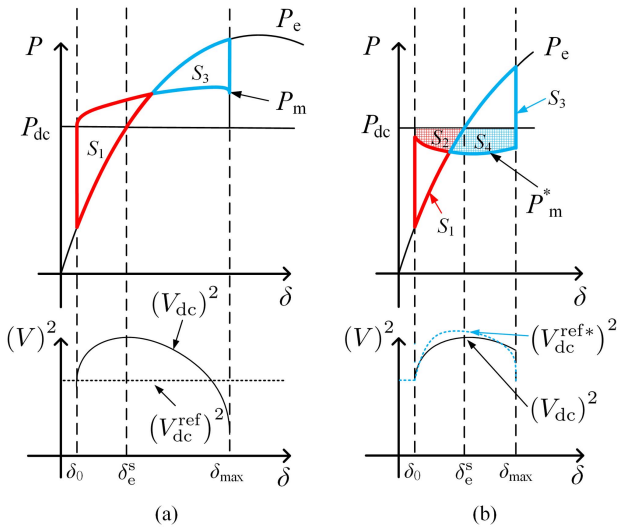

Fig. 8. $P-\delta$ diagram of GFM converter with: (a) DVC and (b) eDVC.

the power angle and the dc-link voltage can be both reduced, thereby alleviating the potential risk of transient instability and dc-link overvoltage protection simultaneously

$$J_p^*\ddot{\delta} = P_{\mathrm{m}}^* - P_{\mathrm{e}} - D_p^*\dot{\delta}$$
$$\begin{cases} P_{\mathrm{m}}^* = P_{\mathrm{m}} - k_{i\mathrm{dc}}k_{\mathrm{d}}\left(\delta - \delta_0\right) \\ J_p^* = J_p - k_{p\mathrm{dc}}k_{\mathrm{dd}} \\ D_p^* = D_p + k_{p\mathrm{dc}}k_{\mathrm{d}} - k_{i\mathrm{dc}}k_{\mathrm{dd}}. \end{cases} \tag{12}$$

The introduction of loop (I) increases the virtual damping while decreasing the magnetic power. The more significantly the magnetic power and damping adjusted, the better the transient stability of the GFM converter [14]. However, the design of its parameter k_{d} should guarantee that adjusted $V_{\mathrm{dc}}^{\mathrm{ref}}$ will not exceed its protection constraints. Loop (II) decreases the virtual inertia but also compromises the effect of damping enhancement. Therefore, the design of its parameter k_{dd} should satisfy $k_{i\mathrm{dc}}k_{\mathrm{dd}} < k_{p\mathrm{dc}}k_{\mathrm{d}}$ to guarantee the change of damping to be positive.

To avoid the reduction of virtual inertia during normal operation caused by loop (II), a fault detection block is incorporated into the eDVC, as shown in Fig. 7, where δ_0 denotes the initial point of the power angle during normal operation, δ_{th} and E_{th} denote the threshold of the power angle and output voltage respectively. The fault detection block uses local δ and E_{ref} of VSG to detect the occurrence of fault, avoiding difficulties in obtaining system parameters, such as voltage amplitude or phase angle of the point of common coupling. The output active power of the GFM converter experiences sudden change in both grid voltage drop and phase jump faults, according to (4), the mismatch of the output active power and its reference causes the power angle to exceed its initial point during steady-state operation. Therefore, a power angle-based fault detection block, which compares the power angle δ obtained locally with its stable operating range $\delta_0 \pm \delta_{\mathrm{th}}$, is employed to accurately activate eDVC and ensure the safe deactivation of eDVC until the synchronization is recovered after fault clearing. Furthermore, the output reactive power will also experience sudden increase at fault instant, according to (5). Due to the fast response of the first order $Q-V$ droop characteristic, the converter output voltage reference will be decreased instantaneously at the moment of the fault occurrence as the result of the sudden change in reactive power. Therefore, an output voltage-based fault detection block, which compares the difference between the reference value of the output voltage of the converter E_{ref} and its rated value E_n with the threshold E_{th}, is employed to ensure the prompt activation of eDVC.

The effectiveness of the proposed eDVC is further demonstrated through the perspective of the energy function, with the adjusted energy function due to the introduction of eDVC provided in the appendix. By employing eDVC, the attraction region of the system is expanded, as depicted in Fig. 9(a) and (b), by enabling the dc-link capacitor to store unbalanced power and decreasing the converter's inertia. This expansion ensures that the system's initial operating point falls within the attraction region, thereby preventing transient instability caused by the system energy exceeding the critical energy. As shown by the two system trajectories on the $\delta-\omega$ plane in Fig. 9(c), when the converter systems operate with the same dc-side input power and voltage drop level—i.e., starting from the same initial operating point—the system utilizing eDVC exhibits an initial energy lower than the critical energy, enabling it to eventually stabilize at the SEP. In contrast, the system employing conventional DVC has an initial energy exceeding the critical energy, leading to a continuous increase in kinetic energy and ultimately resulting in LOS. Furthermore, due to the introduction of eDVC, the damping effect of the converter is enhanced, effectively mitigating the negative damping area, as illustrated in Fig. 9(d). This adjustment alleviates the risk of the attraction region disappearing due to negative damping effects.

B. Cost-Effective Design Consideration

To investigate the relationship between the grid voltage fault depth and the dc-link voltage elevation, analytical results are presented in Fig. 10, with a fault duration of 625 ms, where

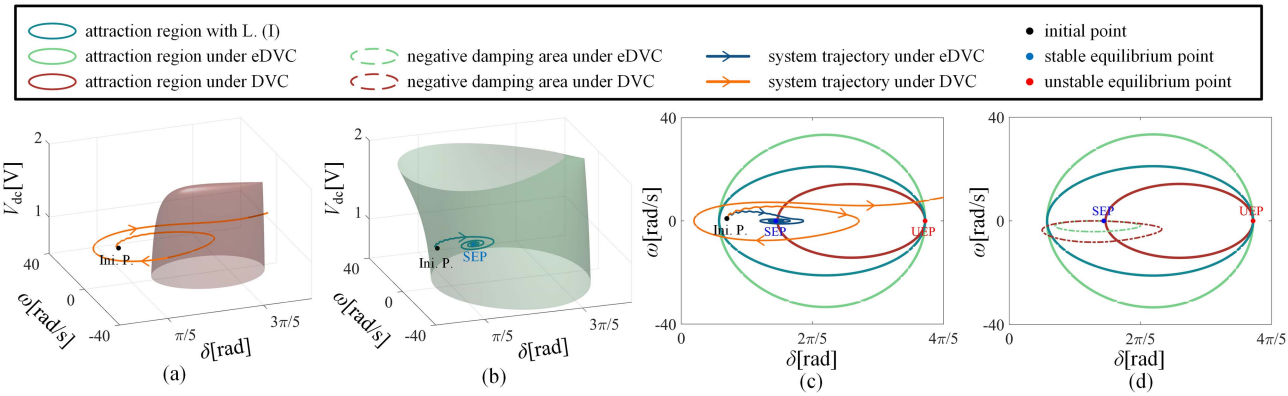

Fig. 9. Attraction region during transient. (a) DVC. (b) eDVC. (c) $\delta - \omega$ plane. (d) Negative damping area.

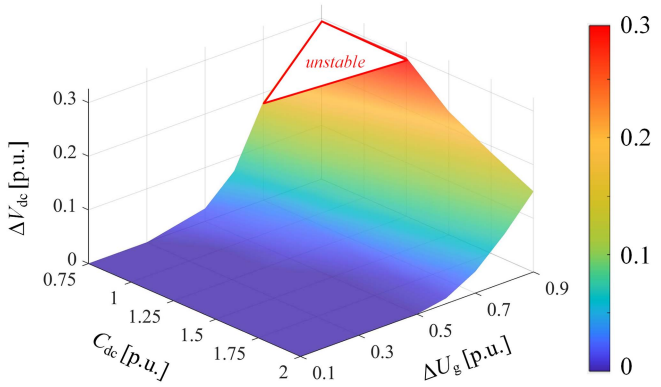

Fig. 10. Required elevation of DC-link voltage for the converter to maintain stability under different DC-link capacitors and fault depths.

$\Delta V_{\rm dc}$ indicates the additional dc-link voltage elevation at SEP achieved by eDVC compared to the conventional DVC. As shown in Fig. 10, the use of eDVC expands the stability region of the GFM converter. Furthermore, with deeper grid voltage sag $\Delta U_{\rm g}$, a higher extent of dc-link voltage elevation is required to maintain system stability, indicating that the dc-link capacitor needs to temporarily store greater levels of unbalanced power to prevent system from instability. To further demonstrate the effectiveness of eDVC with different capacitances of the dc-link capacitor, more detailed experimental results are presented as follows. When the allowable increase in dc-link voltage is limited to 0.2 p.u., maintaining synchronization during a 0.9 p.u. fault only requires increasing the capacitance of dc-link capacitor to 1.75 p.u. This value is significantly lower than that of a supercapacitor, resulting in a much lower cost. Moreover, even if the capacitance cannot be increased and remains at 1 p.u., employing eDVC still results in a 55.2% increase in the critical clearing time under a 0.9 p.u. voltage drop fault, significantly enhancing the stability metric of the converter. Therefore, the eDVC method does not solely rely on high-value capacitors. In contrast, it reduces the required capacitance for the system's stability or improves stability metric under any dc-link capacitor.

Building on the fact that the eDVC strategy does not rely on high-value capacitors, another key advantage of this method lies in its implementation simplicity. The eDVC strategy is a cost-effective add-on control [40] that utilizes signals from the existing GFM control interfaces, such as the power angle of the converter, and the amplitude of the output voltage. Consequently, it requires no additional hardware interfaces or modifications to the original GFM control structure. Instead, the implementation involves only software modifications, significantly reducing system complexity and costs while enhancing the system's stability. Compared to cost-intensive hardware-based solutions, such as the integration of supercapacitor [41], the eDVC strategy offers a practical, efficient, and scalable approach to improving system transient stability.

C. Consideration of Current Limiter

To prevent converters from overcurrent tripping, circular current limiter is adopted. This section discusses the effectiveness of eDVC considering current limiter.

The expression of current limiter is as follows [43]:

$$\bar{I}^{\rm ref}_{{\rm f},dq} = \sigma I^{\rm ref}_{{\rm f},dq}, \quad \sigma = \min\left\{1, \frac{I_M}{\|I^{\rm ref}_{{\rm f},dq}\|}\right\} \tag{13}$$

where $I^{\rm ref}_{{\rm f},dq}$ is the original current reference generated by the voltage control loop, as shown in Fig. 11. $\bar{I}^{\rm ref}_{{\rm f},dq}$ is the saturated current reference, and I_M is the maximum allowable converter side current magnitude. Only the magnitude of current reference is decreased when the magnitude current limiter is triggered, while its angle is kept unchanged.

When the circular current limiter is triggered, the voltage integral controller is kept at zero during the current limiting period avoid the integrator windup. The expression of $I_{{\rm f},dq}$ can be rewritten as

$$\begin{aligned} I_{{\rm f},dq} &= \sigma K_{pV}\left(E^{\rm ref}_{dq} - E_{dq}\right) + \sigma I_{{\rm f},dq} \\ &\Rightarrow R_e I_{{\rm f},dq} = E^{\rm ref}_{dq} - E_{dq} \end{aligned} \tag{14}$$

where $R_e = \frac{1-\sigma}{\sigma K_{pV}}$ is a positive real variable.

Therefore, the inner control loop with the circular current limiter can be represented as a voltage source behind equivalent resistance R_e [42], as shown in Fig. 11. Take the virtual resistance into consideration, the output active power of the converter

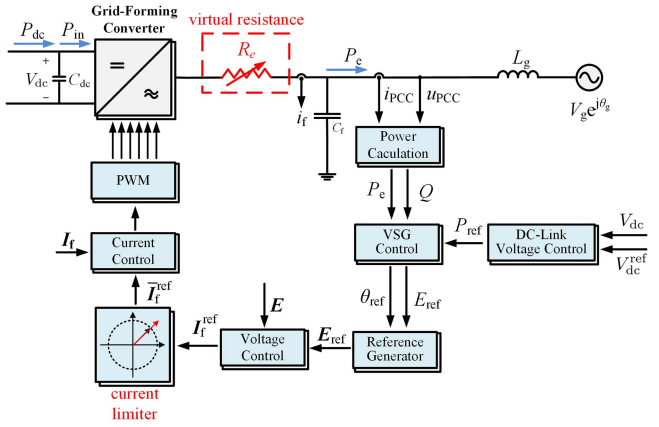

Fig. 11. System configuration of the GFM converter considering current limiter [42].

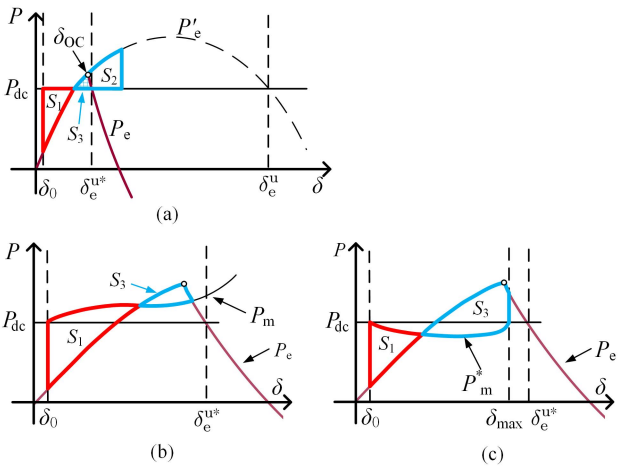

Fig. 12. $P-\delta$ diagram of GFM converter considering: (a) current limiter, (b) current limiter and DVC, and (c) current limiter and eDVC.

should be modified to

$$P_e = \frac{3}{2}\left(\frac{\omega_n L_g}{(R_e)^2+(\omega_n L_g)^2}E_{\text{ref}}V_g\sin\delta + \frac{R_e}{(R_e)^2+(\omega_n L_g)^2}\left((E_{\text{ref}})^2 - E_{\text{ref}}V_g\right)\cos\delta - I_M^2 R_e\right) \tag{15}$$

where $R_e = \max\{0, \text{Re}(\bar{R}_e)\}$ with

$$\bar{R}_e = \sqrt{\frac{(E_{\text{ref}})^2 - 2E_{\text{ref}}V_g\cos\delta + V_g^2}{I_M^2} - \omega_n^2 L_g^2}. \tag{16}$$

The $P-\delta$ figure of the GFM converter considering current limiter is shown in Fig. 12(a). As illustrated in the figure, the primary impact of the current limiter on the transient stability of the converter is the reduction of the converter's output active power after the overcurrent point δ_{OC}, as the red solid line shown in Fig. 12(a). This reduction sways the UEP from $\delta_{\text{e}}^{\text{u}}$ to $\delta_{\text{e}}^{\text{u}*}$, leading to the decrease of decelerating area from S_2 to S_3,

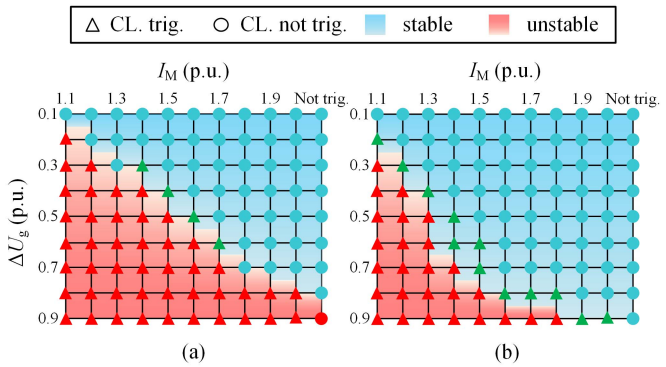

Fig. 13. Stable region of the GFM converter considering current limiter and employing: (a) DVC and (b) eDVC.

thereby impairing the transient stability. By incorporating the proposed eDVC, the unbalanced power is temporarily stored in the dc-link capacitor. As a result, even when the current limiter is triggered, the reduction in active power reference caused by the eDVC effectively decreases the accelerating area and increases the decelerating area, as shown in Fig. 12(b) and (c), thereby preventing the power angle from exceeding the UEP.

To further investigate the impact of current limiter on the effectiveness of eDVC, comparison study under a 325 ms fault has been conducted and the results are shown in Fig. 13, where red triangle symbols ▲ denote the operating regime that current limiter is triggered and the converter loses its stability, blue round symbols • denote the operating regime that current limiter is not triggered and the converter keeps its stability, and green triangle symbols ▲ denote the operating regime that current limiter is triggered while the converter can still remain synchronization. It can be seen from Fig. 13(a), smaller maximum allowable current I_M undoubtedly makes the current limiter easier to be triggered, and results in the reduction of stable region. When the eDVC is introduced, even if the maximum elevation of dc-link voltage is limited to 0.1 p.u., it can still significantly enlarge the stable region of the converter. For instance, as shown in Fig. 13(b), when I_M is set to 1.7 p.u., the maximum fault depth at which the converter can remain stable increases from 0.6 p.u. to 0.85 p.u., indicating that the resilience of converter to disturbances is improved. Meanwhile, eDVC helps prevent overcurrent protection from triggering. For instance, the maximum fault depth that the output current does not reach its saturation increases from 0.55 p.u. to 0.8 p.u. when the saturation I_M is set to 1.7 p.u.. Furthermore, even when the current limiter is already triggered, namely, the power angle has exceeded the overcurrent point δ_{OC}, eDVC can prevent the power angle from further surpassing the UEP by expanding the decelerating area. Finally, as illustrated in Fig. 14, a smaller maximum allowable current I_M requires higher elevation of dc-link voltage to maintain synchronization of the converter.

D. Comparison With Existing Control Methods

The advantages and limitations of existing control methods [44], [45], [46], [36], [47], [48] are summarized in Table III.

TABLE III
COMPARISON OF PROPOSED EDVC AND EXISTING STABILITY ENHANCEMENT CONTROL METHODS

Stability enhancement control	Advantages	Limitations
Transient damping method [44], [45]	· alleviate the risk of overcurrent · add-on control	· exacerbate the risk of overvoltage · rely on phase lock loop · affect dynamics under steady-state operation
Output voltage regulation and reactive power injection [46]	· no impact on dc-link voltage dynamic · no additional control loop	· exacerbate the risk of overcurrent · rely on the measurement of line impedance
Active power regulation [36], [47]	· add-on control	· exacerbate the risk of overvoltage · rely on measurement of grid voltage
Frequency feedback control [48]	· alleviate the risk of overcurrent · uses local information	· exacerbate the risk of overvoltage · noise sensitive
Enhanced DVC	**· alleviate the risk of overvoltage, overcurrent and LOS · add-on control, uses local information · no impact on dynamics under steady-state operation**	**· interaction between two control blocks**

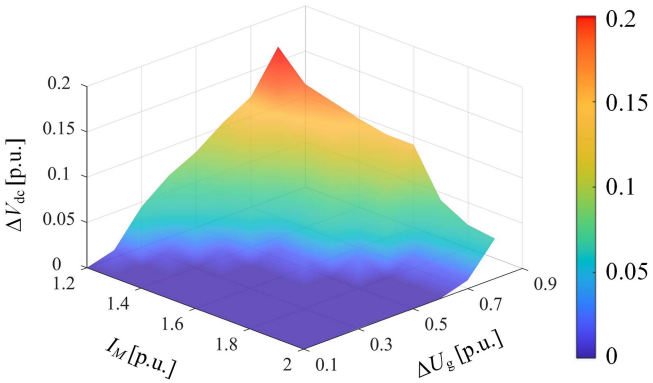

Fig. 14. Required elevation of DC-link voltage for the converter to maintain stability under different maximum allowable current and fault depth.

TABLE IV
EXPERIMENTAL PARAMETERS I

Symbol	Description	Value
J_p, D_p	VSG control parameters	1 p.u., 1 p.u.
$k_{\rm d}, k_{\rm dd}$	eDVC control parameters	60000, 4000

Compared with the above-mentioned stability enhancement control methods, eDVC alleviates both the risks of overvoltage, overcurrent, and LOS simultaneously. Meanwhile, the proposed control employs add-on design and only uses local information of the converter for fault detection, making it easy to implement in practice. Furthermore, due to the existence of fault detection block, eDVC has no impact on the dynamics under steady-state operations, ensures the converter to provide sufficient inertia and voltage support. The main limitation of eDVC is that it requires signal exchanges between DVC and VSG control block.

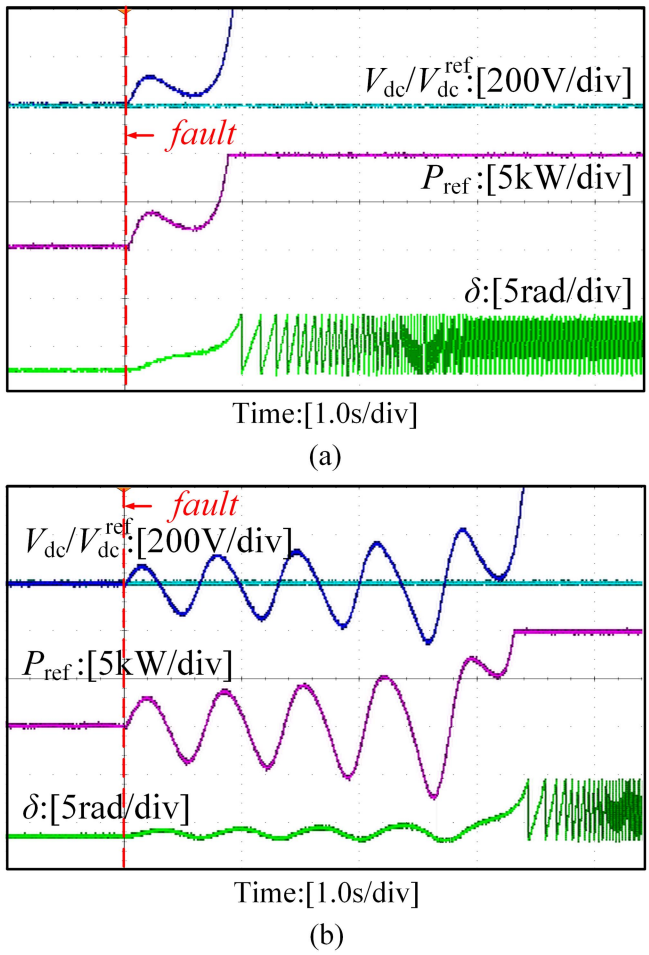

Fig. 15. Experimental results. (a) Grid voltage drops to 0.48 p.u. (b) Grid voltage drops to 0.6 p.u. with $k_{i\rm dc}$ set to 8 p.u.

V. EXPERIMENTAL VALIDATION

To verify the effectiveness of the proposed energy function-based stability analysis method and eDVC, a hardware-in-loop-based experimental platform via RT-box has been developed.

Fig. 15(a) shows the detailed experimental results using parameters listed in Table IV when the grid voltage drops to 0.48 p.u.. When using the traditional DVC, GFM converter fails to maintain synchronization, causing $V_{\rm dc}$ (the deep blue line) to exceed its upper limit. Fig. 16(a) illustrates the corresponding experimental trajectories and the boundary of attraction region. When the dc-link effect is not considered, the initial point of the system is located within the attraction region, indicating that the GFM converter will maintain synchronization during the large disturbance, which contradicts the experimental results. Conversely, when the dc-link effect is taken into account, the attraction region of the system reduces to the blue region in

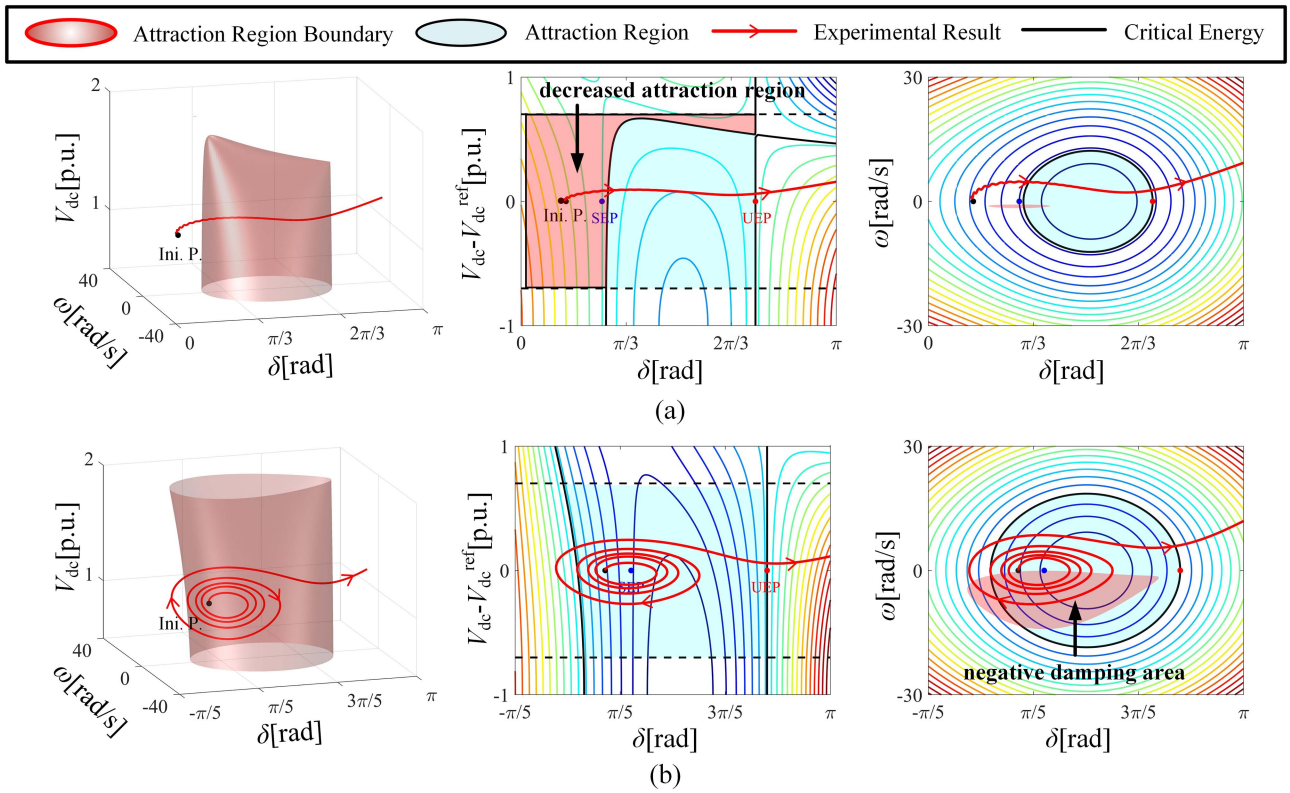

Fig. 16. Attraction region during transient. (a) Grid voltage drops to 0.48 p.u. (b) Grid voltage drops to 0.48 p.u. with $k_{i\mathrm{dc}}$ set to 8 p.u.

Fig. 16(a), resulting in the initial point being outside the attraction region and LOS, aligning with the experimental results. Fig. 15(b) shows the experimental results when the grid voltage drops to 0.6 p.u., with the integral coefficient gain of DVC set to 8 p.u. Negative damping phenomenon is found in this operating regime, as the power angle exhibits oscillatory behavior where the amplitude of subsequent cycles larger than that of the first swing period, indicating the system energy is accumulating rather than dissipating. Fig. 16(b) illustrates the corresponding experimental trajectories and the boundary of attraction region. It can be observed that even if the initial point is located within the attraction region, negative damping effect can cause the increase of system energy, thus leading to transient instability. Overall, ignoring dc-link effect or negative damping effect can either lead to overly optimistic stability assessment.

To validate the effectiveness of the proposed eDVC, experiments were conducted using parameters listed in Table IV under a grid voltage drop to 0.48 p.u. It can be seen in Fig. 17, when a voltage drop fault occurs, the output voltage reference experiences an instantaneous drop, causing the error to exceed its threshold, thereby triggering the fault detection block and activating the eDVC. Due to the instantaneous response of first-order reactive droop control loop, the grid fault can be detected with about three quarters of a cycle, ensuring the timely activation of eDVC. As Fig. 18(a) shows, when the control loop (I) is applied, the $V_{\mathrm{dc}}^{\mathrm{ref}}$ (the light blue line) is elevated during fault, leading to a faster increase in the dc-link voltage compared to traditional control, enabling the dc-link capacitor to temporarily store the unbalanced power. As a result, the increase in P_{m} caused by DVC is effectively avoided, even making it less than P_{dc} during fault, thus enabling the GFM converter to maintain synchronization with the grid. Furthermore, as Fig. 18(b) and (c) shows, by implementing control loop (II), the transient dynamics of the converter is fastened, thus reducing the overshoot of the dc-link voltage by 13.4% and the power angle by 14.6%, resulting in improved transient stability. The results validate the effectiveness of the proposed control strategy.

TABLE V
DYNAMIC CHARACTERISTICS

	DVC	eDVC	change rate
overshoot of dc-link voltage $\sigma_V[\%]$	7	7.27	3.86%
setting time of dc-link voltage $t_{sV}[s]$	1.08	0.32	-70.37%
overshoot of power angle $\sigma_\delta[\%]$	37.3	19.55	-47.59%
setting time of power angle $t_{s\delta}[s]$	3.13	0.52	-83.39%

Fig. 19 presents the experimental results when the grid voltage drops to 0.65 p.u., aimed at investigating the impact of eDVC on the dynamic characteristics of the dc-link voltage and power angle of the GFM converter. According to the results listed in Table V, the proposed eDVC reduces the setting time of dc-link voltage by 70.37%, from t_{sV} to t_{sV}^{*} shown in Fig. 19(c), while only causing a 3.86% increase in the dc-link voltage overshoot. The duration of the dc-link voltage exceeding its reference value

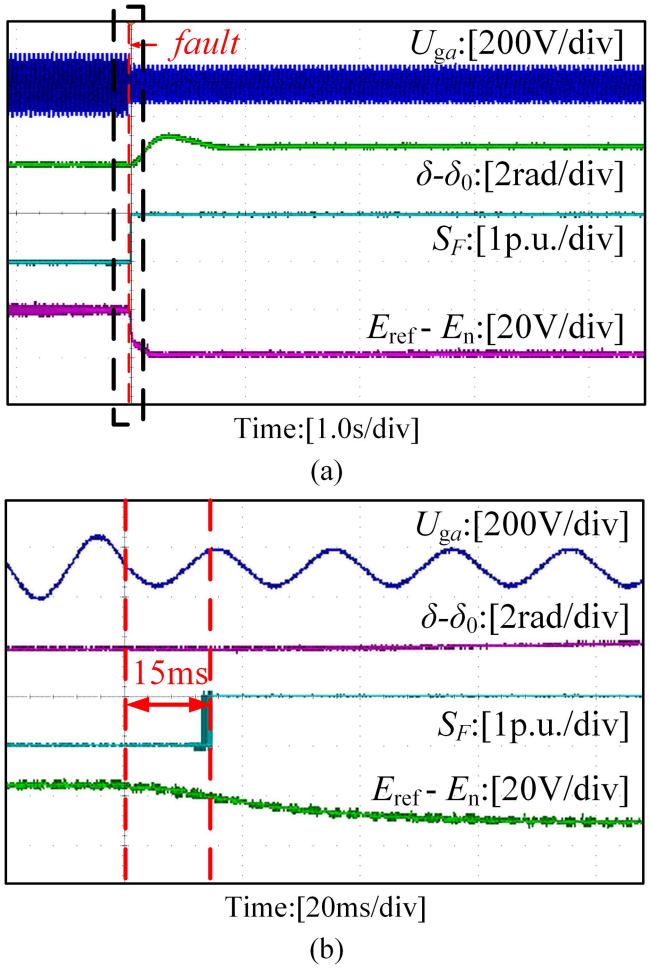

Fig. 17. Experimental results when grid voltage drops to 0.48 p.u. (a) Fault detection block. (b) Zoomed scope.

TABLE VI
EXPERIMENTAL PARAMETERS II

Symbol	Description	Value
I_M	Maximum allowable current magnitude	1.22 p.u.
J_p, D_p	VSG control parameters	1.5 p.u., 2 p.u.
$k_{\rm d}$, $k_{\rm dd}$	eDVC control parameters	80000, 6000

is significantly shortened, thereby reducing energy consumption on the dc-link side and lowering the system's operating cost. Furthermore, the overshoot and setting time of the power angle are reduced by 47.59% and 83.39%, respectively, greatly improving the dynamic performance of the GFM converter during transient faults and enhancing the transient stability of the converter.

To investigate the effectiveness of the proposed eDVC under the scenario that the converter is facing the risk of overcurrent during transient, the experiment considers both current limiter and dc-link dynamic is conducted. The grid voltage drops to 0.6 p.u. during fault and other system parameters are listed in Table VI. It can be observed from Fig. 20(a) that when using the conventional DVC, the dc-link voltage rises rapidly after the current limiter is triggered due to the decrease in the converter's

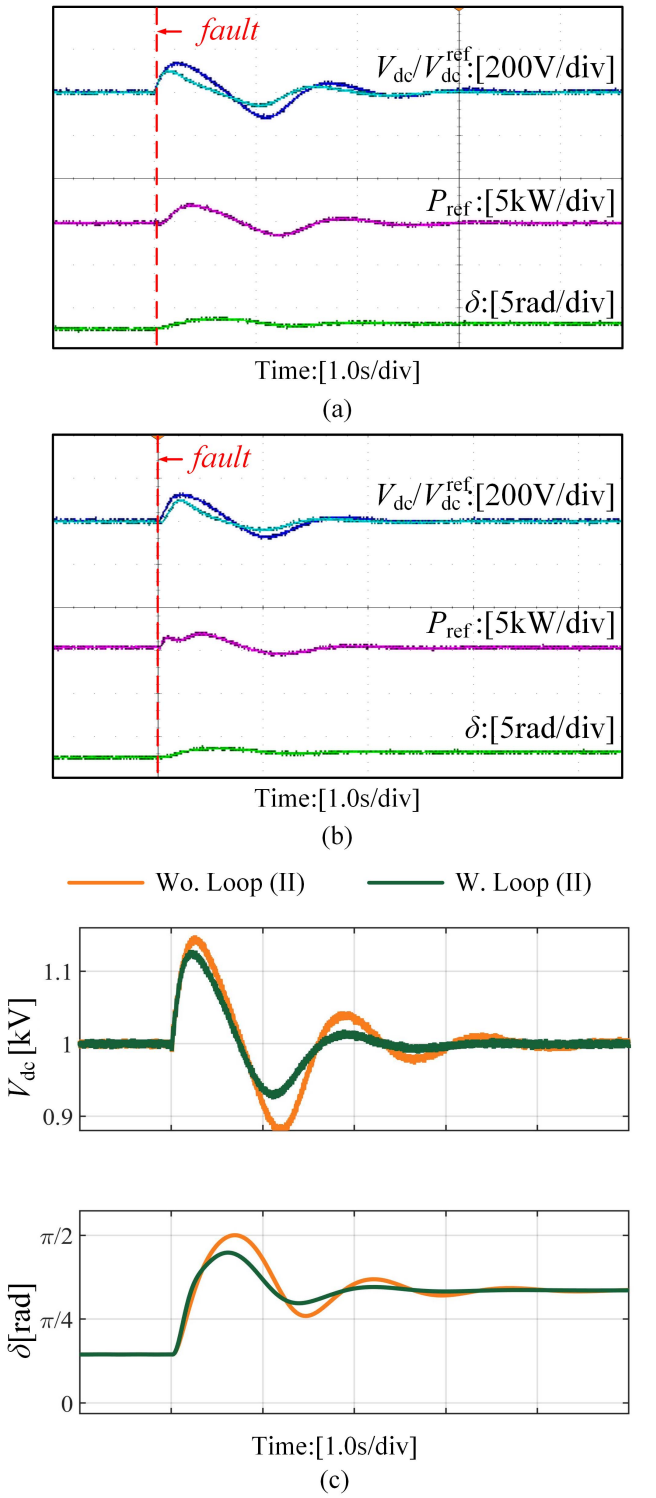

Fig. 18. Experimental results when grid voltage drops to 0.48 p.u. (a) eDVC with Loop (I). (b) eDVC with Loop (I) and Loop (II). (c) Comparison.

output active power. This leads to an increase in the dc-link voltage and active power reference, which subsequently enlarges the accelerating area and reduces the decelerating area, causing a rapid increase in the power angle. This, in turn, results in a

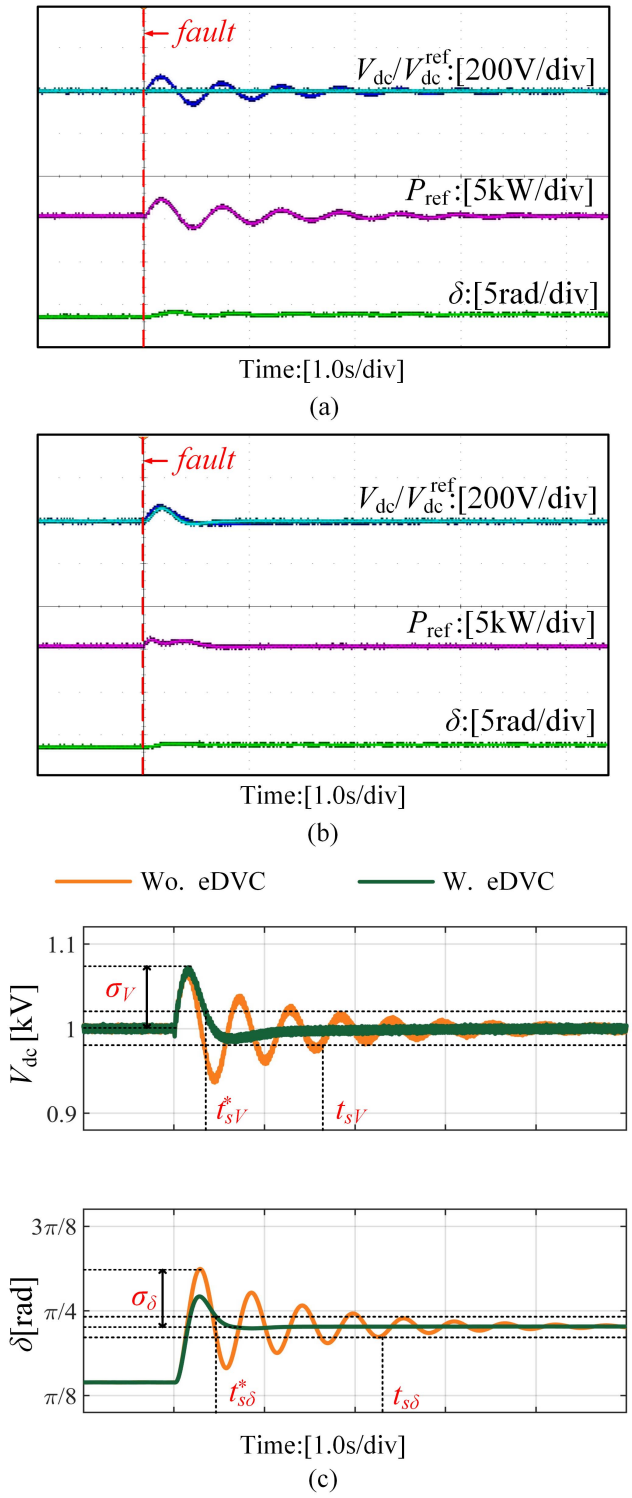

Fig. 19. Experimental results when grid voltage drops to 0.65 p.u. (a) DVC. (b) eDVC. (c) Comparison.

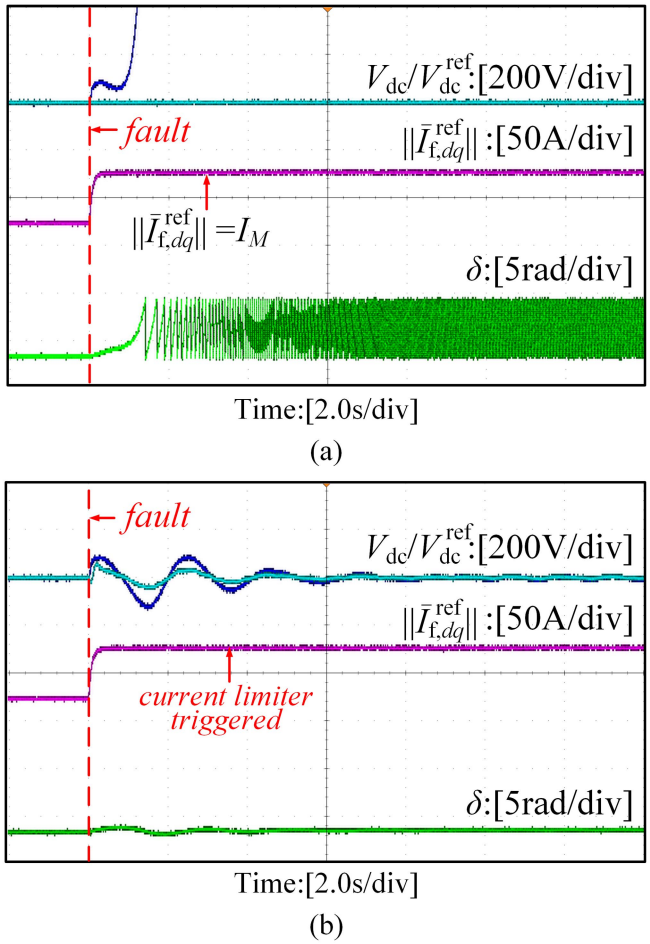

Fig. 20. Experimental results when grid voltage drops to 0.6 p.u. with current limiter triggered. (a) DVC. (b) eDVC.

further decrease in output power, ultimately leading to converter instability. Meanwhile, as shown in Fig. 20(b), when eDVC is employed, the adjustment in the dc-link voltage reference value reduces the accelerating area and increases the decelerating area, thereby preventing the power angle from exceeding UEP.

VI. Conclusion

In this article, the impact of DVC and parametric effect on the transient stability of the GFM converter is analyzed from the perspective of Lyapunov direct method and invariance principle. The potential energy distribution reveals that the effect of DVC decreases the attraction region of GFM converter, which may result in initial energy larger than critical energy and transient instability in consequence. Meanwhile, DVC and inappropriate control parameters can introduce negative damping effect to the system, which may cause attraction region disappearing even when the initial energy is smaller than critical energy. To solve this problem, an enhanced DVC for transient stability improvement is proposed, which enables dc-link capacitor to temporarily store the unbalanced power between dc and ac side, expanding the attraction region and alleviating negative damping effect, while also decreasing the virtual inertia to accelerate the converging process and thereby alleviate the risk of dc-link overvoltage. The implementation of eDVC can extend the system's maximum fault clearing time by 55.17% under severe fault condition. When current limiter is considered, the maximum fault depth that leads to overcurrent and transient instability can be extended by 25% simultaneously. Furthermore, the setting

time of the power angle and dc-link voltage can be decreased by 70.37% and 83.39%, and the overshoot of the power angle can be decreased by 47.59%, with only a 3.86% increase in the overshoot of dc-link voltage. Experimental results have validated the effectiveness of the proposed energy function and control strategy.

APPENDIX

A Construction of the Energy Function

There are two main concerns once employing traditional SG-like transient energy function of the system, whose expression is as follows:

$$\begin{aligned}\mathbf{V} &= \frac{1}{2}J_p\Delta\omega^2 - P_{\text{ref}}\delta - EV_{\text{g}}B_{\text{g}}\cos\delta \\ &= \frac{1}{2}J_p\Delta\omega^2 - EV_{\text{g}}B_{\text{g}}\cos\delta \\ &\quad - \left(P_{\text{dc}} + \left(k_{p\text{dc}} + k_{i\text{dc}}\int\right)\left((V_{\text{dc}})^2 - \left(V_{\text{dc}}^{\text{ref}}\right)^2\right)\right)\delta\end{aligned} \tag{A.1}$$

$$\begin{aligned}\dot{\mathbf{V}} &= J_p\ddot{\delta}\dot{\delta} - P_{\text{ref}}\dot{\delta} + EV_{\text{g}}B_{\text{g}}\sin\delta\dot{\delta} - \dot{P_{\text{ref}}}\delta \\ &= -D_p\Delta\omega^2 \\ &\quad - \underbrace{\left(k_{i\text{dc}}\cdot\left((V_{\text{dc}})^2 - \left(V_{\text{dc}}^{\text{ref}}\right)^2\right) + \frac{2k_{p\text{dc}}}{C_{\text{dc}}}\cdot(P_{\text{dc}} - P_{\text{e}})\right)\delta}_{\text{DVC interaction}}.\end{aligned} \tag{A.2}$$

First, with the introduction of DVC, P_{ref} in the energy function is no longer a constant but a function of time rather than state variables. This change makes it impossible to calculate the value of P_{ref} in the energy function. Second, the interaction term introduced by DVC causes the region where the derivative of the energy-like Lyapunov function is positive to become unbounded, thereby rendering the energy function incompatible with the extended invariance principle. Therefore, two corresponding modifications to the energy function are made: first, for the interaction term introduced by the proportional coefficient $k_{p\text{dc}}$, considering the relationship

$$P_{\text{dc}} - P_{\text{e}} = EV_{\text{g}}B_{\text{g}}\left(\sin\delta - \sin\delta_{\text{e}}^{\text{s}}\right) \tag{A.3}$$

an adjusting function was constructed to ensure that it has opposite polarity to $P_{\text{dc}} - P_{\text{e}}$. By multiplying adjusting function and power difference, the negative damping area can be guaranteed bounded

$$f_{\text{ad}}(\delta) = \left(-\delta + \zeta\sin\left(\frac{\pi}{2}\frac{\delta - \delta_{\text{e}}^{\text{s}}}{\delta_{\text{e}}^{\text{u}} - \delta_{\text{e}}^{\text{s}}}\right) + \delta_{\text{e}}^{\text{s}}\right). \tag{A.4}$$

Second, to avoid the appearance of integral coefficient $k_{i\text{dc}}$ in the energy function, the replacement of time-dependent function to state variables-dependent function has been made.

By substituting (1) and (3) into (6), (6) can be rewritten as

$$\begin{aligned}\frac{\text{d}}{\text{d}t}\Delta V_{\text{dc}}^2 &= \frac{4}{C_{\text{dc}}}(P_{\text{dc}} - P_{\text{e}}) \\ &= \frac{4}{C_{\text{dc}}}(P_{\text{ref}} - P_{\text{e}} + P_{\text{dc}} - P_{\text{ref}}) \\ &= \frac{4}{C_{\text{dc}}}\left(J_p\ddot{\delta} + D_p\dot{\delta} - \left(k_{p\text{dc}} + k_{i\text{dc}}\int\right)\Delta V_{\text{dc}}^2\right)\end{aligned} \tag{A.5}$$

where $\Delta V_{\text{dc}}^2 = ((V_{\text{dc}})^2 - (V_{\text{dc}}^{\text{ref}})^2)$, (A.5) can be rewritten as

$$\left(k_{i\text{dc}}\int + k_{p\text{dc}} + \frac{C_{\text{dc}}}{4}\frac{d}{\text{d}t}\right)\Delta V_{\text{dc}}^2 = \left(J_p\ddot{\delta} + D_p\dot{\delta}\right). \tag{A.6}$$

To avoid introducing higher order dynamics, the integral term is ignored. Take the integration of (A.6), whose expression is

$$\int\Delta V_{\text{dc}}^2\text{d}t = \frac{1}{k_{p\text{dc}}}\left(\left(J_p\dot{\delta} - D_p\left(\delta - \delta_{\text{e}}^{\text{s}}\right)\right) - \frac{C_{\text{dc}}}{4}\Delta V_{\text{dc}}^2\right). \tag{A.7}$$

Therefore, the time-dependent term in the energy function can be replaced by state-variables-dependent term.

B Seminegative Definite of dV/dt

The negativeness of time derivative of the derived energy function (8) can be proved by using chain rule for partial derivatives, which can be evaluated as follows:

$$\begin{aligned}\dot{\mathbf{V}}(\omega,\delta,V_{\text{dc}}) &= \frac{\partial\mathbf{V}}{\partial\omega}\frac{d\omega}{dt} + \frac{\partial\mathbf{V}}{\partial\delta}\frac{d\delta}{dt} + \frac{\partial\mathbf{V}}{\partial V_{dc}}\frac{dV_{\text{dc}}}{dt} \\ &= J_p\ddot{\delta}\cdot\dot{\delta} - P_{\text{dc}}\cdot\dot{\delta} + EV_{\text{g}}B_{\text{g}}\sin\delta\cdot\dot{\delta} \\ &\quad + k_{p\text{dc}}\left((V_{\text{dc}})^2 - \left(V_{\text{dc}}^{\text{ref}}\right)^2\right)\cdot\dot{\delta} \\ &\quad + \frac{k_{i\text{dc}}}{k_{p\text{dc}}}\left(J\dot{\delta} - D_p\left(\delta - \delta_{\text{e}}^{\text{s}}\right) - \frac{C_{\text{dc}}}{4}\left((V_{\text{dc}})^2 - \left(V_{\text{dc}}^{\text{ref}}\right)^2\right)\right)\cdot\dot{\delta} \\ &\quad + \xi\cdot 2V_{\text{dc}}\dot{V_{\text{dc}}}\left(-\delta + \zeta\sin\left(\frac{\pi}{2}\frac{\delta - \delta_{\text{e}}^{\text{s}}}{\delta_{\text{e}}^{\text{u}} - \delta_{\text{e}}^{\text{s}}}\right) + \delta_{\text{e}}^{\text{s}}\right) \\ &\quad + \xi\cdot\left(\left(V_{\text{dc}}^{\text{ref}}\right)^2 - \left(V_{\text{dc}}^{\text{sat}}\right)^2\right)\cos\left(\frac{\pi}{2}\frac{\delta - \delta_{\text{e}}^{\text{s}}}{\delta_{\text{e}}^{\text{u}} - \delta_{\text{e}}^{\text{s}}}\right)\Delta\omega.\end{aligned} \tag{B.1}$$

By substituting (A.7) into (B.1), the first three row of (B.1) can be rewritten as

$$\begin{aligned}\dot{\mathbf{V}}_1 &= \Big[J_p\ddot{\delta} + P_{\text{dc}} \\ &\quad + \left(k_{p\text{dc}} + k_{i\text{dc}}\int\right)\left((V_{\text{dc}})^2 - \left(V_{\text{dc}}^{\text{ref}}\right)^2\right) \\ &\quad - EV_{\text{g}}B_{\text{g}}\sin\delta\Big]\dot{\delta} \\ &= -D_p\Delta\omega^2.\end{aligned} \tag{B.2}$$

Therefore, the first part of (B.1) is proved to be negative.

For the second part of the (B.1), i.e., the fourth row of (B.1), it can be rewritten into

$$\begin{aligned}\dot{\mathbf{V}}_2 &= 2\xi\cdot V_{\text{dc}}\dot{V_{\text{dc}}}\left(-\delta + \zeta\sin\left(\frac{\pi}{2}\frac{\delta - \delta_{\text{e}}^{\text{s}}}{\delta_{\text{e}}^{\text{u}} - \delta_{\text{e}}^{\text{s}}}\right) + \delta_{\text{e}}^{\text{s}}\right) \\ &= \frac{4\xi}{C_{\text{dc}}}(P_{\text{dc}} - P_{\text{e}})\left(-\delta + \zeta\sin\left(\frac{\pi}{2}\frac{\delta - \delta_{\text{e}}^{\text{s}}}{\delta_{\text{e}}^{\text{u}} - \delta_{\text{e}}^{\text{s}}}\right) + \delta_{\text{e}}^{\text{s}}\right) \\ &= C\left(\sin\delta_{\text{e}}^{\text{s}} - \sin\delta\right)\left(-\delta + \zeta\sin\left(\frac{\pi}{2}\frac{\delta - \delta_{\text{e}}^{\text{s}}}{\delta_{\text{e}}^{\text{u}} - \delta_{\text{e}}^{\text{s}}}\right) + \delta_{\text{e}}^{\text{s}}\right)\end{aligned} \tag{B.3}$$

where $C = 4\xi \cdot EV_{\rm g}B_{\rm g}/C_{\rm dc}$. Obviously, $(\sin\delta_{\rm e}^{\rm s} - \sin\delta)$ is positive for $\delta < \delta_{\rm e}^{\rm s}$ and $\delta > \delta_{\rm e}^{\rm u}$, negative for $\delta_{\rm e}^{\rm s} < \delta < \delta_{\rm e}^{\rm u}$. When ζ is set as $\delta_{\rm e}^{\rm u} - \delta_{\rm e}^{\rm s}$, adjusting function $(-\delta + \zeta\sin(\frac{\pi}{2}\frac{\delta-\delta_{\rm e}^{\rm s}}{\delta_{\rm e}^{\rm u}-\delta_{\rm e}^{\rm s}}) + \delta_{\rm e}^{\rm s})$ can be demonstrated to exhibit opposite definiteness. Therefore, the second part of (B.1) is proven to be negative.

For the third part of (B.1), $(V_{\rm dc}^{\rm ref})^2 - (V_{\rm dc}^{\rm sat})^2$ is always negative, while $\cos(\frac{\pi}{2}\frac{\delta-\delta_{\rm e}^{\rm s}}{\delta_{\rm e}^{\rm u}-\delta_{\rm e}^{\rm s}})$ is positive for $-\delta_{\rm e}^{\rm u} + 2\delta_{\rm e}^{\rm s} < \delta < \delta_{\rm e}^{\rm u}$. Therefore, the dynamic interaction term is negative during the accelerating process of the power angle, which is the primary focus of transient stability.

C Adjustment of Energy Function Facilitated by eDVC

Since the swing equation of the GFM converter with eDVC is modified as (12), the energy function is correspondingly adjusted to

$$\mathbf{V}^* = \frac{1}{2}\left(J_p - k_{\rm pdc}k_{\rm dd}\right)\Delta\omega^2 - P_{\rm dc}\delta - EV_{\rm g}B_{\rm g}\cos\delta - \frac{1}{2}k_{i\rm dc}k_{\rm d}\left(\delta-\delta_0\right)^2 + \ldots \tag{C.1}$$

$$\dot{\mathbf{V}}^* = -\left(D_p + k_{\rm pdc}k_{\rm d} - k_{i\rm dc}k_{\rm dd}\right)\Delta\omega^2 + \ldots. \tag{C.2}$$

REFERENCES

[1] Z. Zou, J. Tang, G. Buticchi, and M. Liserre, "Stabilization of distribution grids with high penetration of renewables: The path from decentralized control to a centralized one," *IEEE Ind. Electron. Mag.*, vol. 18, no. 1, pp. 17–31, Mar. 2024.

[2] J. M. Guerrero et al., "Distributed generation: Toward a new energy paradigm," *IEEE Ind. Electron. Mag.*, vol. 4, no. 1, pp. 52–64, Mar. 2010.

[3] H. Zhang, W. Xiang, W. Lin, and J. Wen, "Grid forming converters in renewable energy sources dominated power grid: Control strategy, stability, application, and challenges," *J. Modern Power Syst. Clean Energy*, vol. 9, no. 6, pp. 1239–1256, 2021.

[4] K. Mahmoud, P. Astero, P. Peltoniemi, and M. Lehtonen, "Promising grid-forming VSC control schemes toward sustainable power systems: Comprehensive review and perspectives," *IEEE Access*, vol. 10, pp. 130024–130039, 2022.

[5] J. Rocabert, A. Luna, F. Blaabjerg, and P. Rodriguez, "Control of power converters in AC microgrids," *IEEE Trans. Power Electron.*, vol. 27, no. 11, pp. 4734–4749, Nov. 2012.

[6] J. Liu, Y. Miura, and T. Ise, "Comparison of dynamic characteristics between virtual synchronous generator and droop control in inverter-based distributed generators," *IEEE Trans. Power Electron.*, vol. 31, no. 5, pp. 3600–3611, May 2016.

[7] R. H. Lasseter, Z. Chen, and D. Pattabiraman, "Grid-forming inverters: A critical asset for the power grid," *IEEE Trans. Emerg. Sel. Topics Power Electron.*, vol. 8, no. 2, pp. 925–935, Jun. 2020.

[8] A. Tayyebi, D. Groß, A. Anta, F. Kupzog, and F. Dörfler, "Frequency stability of synchronous machines and grid-forming power converters," *IEEE Trans. Emerg. Sel. Topics Power Electron.*, vol. 8, no. 2, pp. 1004–1018, Jun. 2020.

[9] H.-P. Beck and R. Hesse, "Virtual synchronous machine," in *Proc. 9th Int. Conf. Elect. Power Qual. Utilisation*, 2007, pp. 1–6.

[10] Q.-C. Zhong and G. Weiss, "Synchronverters: Inverters that mimic synchronous generators," *IEEE Trans. Ind. Electron.*, vol. 58, no. 4, pp. 1259–1267, Apr. 2011.

[11] S. D'Arco, J. A. Suul, and O. B. Fosso, "A virtual synchronous machine implementation for distributed control of power converters in smartgrids," *Electr. Power Syst. Res.*, vol. 122, pp. 180–197, 2015.

[12] H. Wu and X. Wang, "Control of grid-forming VSCs: A perspective of adaptive fast/slow internal voltage source," *IEEE Trans. Power Electron.*, vol. 38, no. 8, pp. 10151–10169, Aug. 2023.

[13] D. Pan, X. Wang, F. Liu, and R. Shi, "Transient stability of voltage-source converters with grid-forming control: A design-oriented study," *IEEE Trans. Emerg. Sel. Topics Power Electron.*, vol. 8, no. 2, pp. 1019–1033, Jun. 2020.

[14] J. Lei, X. Xiang, B. Liu, W. Li, and X. He, "Transient stability analysis of grid forming converters based on damping energy visualization and geometry approximation," *IEEE Trans. Ind. Electron.*, vol. 71, no. 3, pp. 2510–2521, Mar. 2024.

[15] J. Fang, Y. Tang, H. Li, and X. Li, "A battery/ultracapacitor hybrid energy storage system for implementing the power management of virtual synchronous generators," *IEEE Trans. Power Electron.*, vol. 33, no. 4, pp. 2820–2824, Apr. 2018.

[16] H. Bevrani, T. Ise, and Y. Miura, "Virtual synchronous generators: A survey and new perspectives," *Int. J. Electr. Power Energy Syst.*, vol. 54, pp. 244–254, 2014.

[17] M. Albu et al., "Measurement and remote monitoring for virtual synchronous generator design," in *Proc. 2010 IEEE Int. Workshop Appl. Meas. Power Syst.*, 2010, pp. 7–11.

[18] J. Guo et al., "Impedance analysis and stabilization of virtual synchronous generators with different DC-link voltage controllers under weak grid," *IEEE Trans. Power Electron.*, vol. 36, no. 10, pp. 11397–11408, Oct. 2021.

[19] L. Harnefors, M. Hinkkanen, U. Riaz, F. M. M. Rahman, and L. Zhang, "Robust analytic design of power-synchronization control," *IEEE Trans. Ind. Electron.*, vol. 66, no. 8, pp. 5810–5819, Aug. 2019.

[20] L. Zhang, L. Harnefors, and H.-P. Nee, "Power-synchronization control of grid-connected voltage-source converters," *IEEE Trans. Power Syst.*, vol. 25, no. 2, pp. 809–820, May 2010.

[21] T. Liu, X. Wang, and F. Liu, "Impact of DC-link voltage control on transient stability of PLL-synchronized voltage-source converters," in *Proc. 2022 Int. Power Electron. Conf.*, 2022, pp. 435–439.

[22] L. Zhao, Z. Jin, and X. Wang, "Transient stability of grid-forming converters with flexible DC-link voltage control," in *Proc. 2022 Int. Power Electron. Conf.*, 2022, pp. 1648–1653.

[23] Z. Yang, R. Ma, S. Cheng, and M. Zhan, "Nonlinear modeling and analysis of grid-connected voltage-source converters under voltage dips," *IEEE Trans. Emerg. Sel. Topics Power Electron.*, vol. 8, no. 4, pp. 3281–3292, Dec. 2020.

[24] C. Luo, T. Liu, X. Wang, and X. Ma, "Design-oriented analysis of DC-link voltage control for transient stability of grid-forming inverters," *IEEE Trans. Ind. Electron.*, vol. 71, no. 4, pp. 3698–3707, Apr. 2024.

[25] M. Kabalan, P. Singh, and D. Niebur, "A design and optimization tool for inverter-based microgrids using large-signal nonlinear analysis," *IEEE Trans. Smart Grid*, vol. 10, no. 4, pp. 4566–4576, Jul. 2019.

[26] C. Shen, W. Gu, W. Sheng, and K. Liu, "Transient stability analysis and design of VSGs with different DC-link voltage controllers," *CSEE J. Power Energy Syst.*, vol. 10, no. 2, pp. 593–604, Mar. 2024.

[27] K. Zhuang, Z. Wang, D. Sun, L. Wu, X. Wang, and H. Xin, "Transient stability analysis and coordination control design for grid-forming PMSG based on dynamics of DC-link capacitor," in *Proc. 2023 IEEE Power Energy Soc. Gen. Meeting*, 2023, pp. 1–5.

[28] Y. Ma et al., "Reduced-order modeling and transient stability analysis of grid-connected VSC in DC-link voltage control timescale," *IEEE Trans. Emerg. Sel. Topics Power Electron.*, vol. 12, no. 3, pp. 2981–2993, Jun. 2024.

[29] C. Luo, X. Ma, T. Liu, and X. Wang, "A flexible saturation limiter for DC-link voltage control of grid-forming inverters with enhanced transient stability," *IEEE Trans. Energy Convers.*, vol. 38, no. 4, pp. 2514–2524, Dec. 2023.

[30] Y. Peng, Z. Shuai, C. Shen, X. Hou, and Z. J. Shen, "Transient stabilization control of electric synchronous machine for preventing the collapse of DC-link voltage," *IEEE Trans. Smart Grid*, vol. 14, no. 1, pp. 82–93, Jan. 2023.

[31] C. Luo, X. Ma, T. Liu, and X. Wang, "Adaptive-output-voltage-regulation-based solution for the DC-link undervoltage of grid- forming inverters," *IEEE Trans. Power Electron.*, vol. 38, no. 10, pp. 12559–12569, Oct. 2023.

[32] H. Khalil, *Nonlinear Control*. New York, NY, USA: Pearson, 2015.

[33] N. Bretas and L. Alberto, "Lyapunov function for power systems with transfer conductances: Extension of the invariance principle," *IEEE Trans. Power Syst.*, vol. 18, no. 2, pp. 769–777, May 2003.

[34] H. Rodrigues, L. Alberto, and N. Bretas, "On the invariance principle: Generalizations and applications to synchronization," *IEEE Trans. Circuits Syst. I. Fundam. Theory Appl.*, vol. 47, no. 5, pp. 730–739, May 2000.

[35] X. Fu, M. Huang, C. K. Tse, J. Yang, Y. Ling, and X. Zha, "Synchronization stability of grid-following VSC considering interactions of inner current loop and parallel-connected converters," *IEEE Trans. Smart Grid*, vol. 14, no. 6, pp. 4230–4241, Nov. 2023.

[36] Z. Shuai, C. Shen, X. Liu, Z. Li, and Z. J. Shen, "Transient angle stability of virtual synchronous generators using Lyapunov's direct method," *IEEE Trans. Smart Grid*, vol. 10, no. 4, pp. 4648–4661, Jul. 2019.

[37] Y. Yuan, J. Ma, S. Wang, P. Wang, and T. Liu, "Transient stability analysis of grid-forming converters during presynchronization process in islanded mode," *IEEE Trans. Power Electron.*, vol. 39, no. 9, pp. 11007–11019, Sep. 2024.
[38] T. Liu, X. Wang, F. Liu, K. Xin, and Y. Liu, "Transient stability analysis for grid-forming inverters transitioning from islanded to grid-connected mode," *IEEE Open J. Power Electron.*, vol. 3, pp. 419–432, 2022.
[39] J. Wang and X. Zhang, "Transient virtual inertia optimization strategy for virtual synchronous generator based on equilibrium point state assessment," *Int. J. Electr. Power Energy Syst.*, vol. 155, 2024, Art. no. 109588.
[40] I. Rusnak and I. Barkana, "Improving performance of PID controllers using adaptive control," in *Proc. 11th IASTED Int. Conf. Control Appl.*, 2009, pp. 252–257.
[41] W. Zheng, K. Ma, and X. Wang, "Hybrid energy storage with supercapacitor for cost-efficient data center power shaving and capping," *IEEE Trans. Parallel Distrib. Syst.*, vol. 28, no. 4, pp. 1105–1118, Apr. 2017.
[42] B. Fan and X. Wang, "Equivalent circuit model of grid-forming converters with circular current limiter for transient stability analysis," *IEEE Trans. Power Syst.*, vol. 37, no. 4, pp. 3141–3144, Jul. 2022.
[43] B. Fan, T. Liu, F. Zhao, H. Wu, and X. Wang, "A review of current-limiting control of grid-forming inverters under symmetrical disturbances," *IEEE Open J. Power Electron.*, vol. 3, pp. 955–969, 2022.
[44] X. Xiong, C. Wu, B. Hu, D. Pan, and F. Blaabjerg, "Transient damping method for improving the synchronization stability of virtual synchronous generators," *IEEE Trans. Power Electron.*, vol. 36, no. 7, pp. 7820–7831, Jul. 2021.
[45] S. Sun et al., "Transient damping of virtual synchronous generator for enhancing synchronization stability during voltage dips," *CES Trans. Electr. Mach. Syst.*, vol. 8, no. 2, pp. 143–151, Jun. 2024.
[46] W. Si and J. Fang, "Transient stability improvement of grid-forming converters through voltage amplitude regulation and reactive power injection," *IEEE Trans. Power Electron.*, vol. 38, no. 10, pp. 12116–12125, Oct. 2023.
[47] S. P. Me, M. H. Ravanji, M. Z. Mansour, S. Zabihi, and B. Bahrani, "Transient stability of paralleled virtual synchronous generator and grid-following inverter," *IEEE Trans. Smart Grid*, vol. 14, no. 6, pp. 4451–4466, Nov. 2023.
[48] J. Yu, X. Lu, S. Xiong, Y. Xing, W. Liu, and J. Yu, "Transient stability enhancement of virtual synchronous generators based on additional frequency control," *IEEE Trans. Emerg. Sel. Topics Power Electron.*, vol. 12, no. 1, pp. 1129–1139, Feb. 2024.

Chenhang Xu (Student Member, IEEE) was born in China, in 2000. He received the B.S. degree in electrical engineering from the Nanjing University of Aeronautics and Astronautics, Nanjing, China, in 2022. He is currently working toward the M.S. degree in electrical engineering with Southeast University, Nanjing, China.

His research focuses on transient stability of power converters.

Zhixiang Zou (Senior Member, IEEE) received the B.Eng. and Ph.D. degrees in electrical and engineering from Southeast University, Nanjing, China, in 2007 and 2014, respectively, and the Dr.-Ing. degree (*summa cum laude*) in power electronics from Kiel University, Kiel, Germany, in 2019.

From 2007 to 2009, he was an Engineer with State Grid Electric Power Research Institute, Nanjing, China. From 2014 to 2019, he was a Research Fellow with the Chair of Power Electronics, Kiel University. He is currently an Associate Professor with the School of Electrical Engineering, Southeast University. His research interests include smart transformers, microgrid stability, modeling and control of power converters.

Dr. Zou is a Member and Industrial Liaison of the IEEE-IES Technical Committee on Renewable Energy Systems, and a Secretary of IEEE Standard P3105. He was the recipient of the Gold Medal in Geneva International Exhibition of Inventions and IEEE PES Outstanding Academic Publishing Award. He is an Associate Editor for IEEE TRANSACTIONS ON INDUSTRIAL ELECTRONICS, IEEE OPEN JOURNAL OF POWER ELECTRONICS, and IEEE ACCESS.

Xinlei Liu (Student Member, IEEE) received the B.S. degree from Hefei City Institute, Hefei, China, in 2021, and the M.S. degree with Yanshan University, Qinhuangdao, China, in 2024, both in electrical engineering. He is currently working toward the Ph.D. degree in electrical engineering with Southeast University, Nanjing, China.

His research interests include the stability of power converters, modular multilevel converter, multibus multiport energy router, and solid state transformer insulation.

Meng Huang (Member, IEEE) received the B.Eng. and M.Eng. degrees from the Huazhong University of Science and Technology, Wuhan, China, in 2006 and 2008, respectively, and the Ph.D. degree in power electronics from the Hong Kong Polytechnic University, Hong Kong, 2013.

He is currently a Professor with the School of Electrical Engineering and Automation, Wuhan University, Wuhan, China. His research interests include safe operation and control of grid-connected systems.

Dr. Huang was the recipient of the Best Paper Award of the IEEE TRANSACTIONS ON POWER ELECTRONICS in 2016, and the Excellent Paper Award of *CSEE Journal of Power and Energy System*. He is an Editor for the *International Journal of Circuit Theory and Applications*, and was a Guest Editor for IEEE JOURNAL OF EMERGING AND SELECTED TOPICS OF CIRCUITS AND SYSTEMS, and the Guest Associate Editor for IEEE TRANSACTIONS ON INDUSTRIAL APPLICATIONS and IEEE JOURNAL OF EMERGING AND SELECTED TOPICS OF POWER ELECTRONICS.

Wu Chen (Senior Member, IEEE) was born in Jiangsu, China, in 1981. He received the B.S., M.S., and Ph.D. degrees in electrical engineering from the Nanjing University of Aeronautics and Astronautics, Nanjing, China, in 2003, 2006, and 2009, respectively.

From 2009 to 2010, he was a Senior Research Assistant with the Department of Electronic Engineering, City University of Hong Kong, Hong Kong. In 2010 and 2011, he was a Postdoctoral Researcher with Future Electric Energy Delivery and Management Systems Center, North Carolina State University, Raleigh, NC, USA. Since September 2011, he has been an Associate Research Fellow with the School of Electrical Engineering, Southeast University, Nanjing, China, where he has been a Professor since 2016. His research interests include soft-switching converters, power delivery, and power electronic system integration.

Dr. Chen is an Associate Editor for IEEE TRANSACTIONS ON INDUSTRIAL ELECTRONICS, *Journal of Power Electronics*, and *CPSS Transactions on Power Electronics and Applications*.

Zheng Wang (Senior Member, IEEE) received the B.Eng. and M.Eng. degrees from Southeast University, Nanjing, China, in 2000 and 2003, respectively, and the Ph.D. degree from the University of Hong Kong, Hong Kong, in 2008, all in electrical engineering.

From 2008 to 2009, he was a Postdoctoral Fellow with Ryerson University, Toronto, ON, Canada. He is currently a Full Professor with the School of Electrical Engineering, Southeast University. In these fields, he has authored more than 120 internationally refereed papers, one English book by IEEE-Wiley Press, and two English book chapters. His research interests include electric drives, power electronics, and distributed generation.

Dr. Wang was the recipient of IEEE PES Chapter Outstanding Engineer Award, First-class Science and Technology Award of Jiangsu Province in China, and Outstanding Young Scholar Award of Jiangsu Natural Science Foundation of China. He is an IET Fellow and an Associate Editor for IEEE TRANSACTIONS ON INDUSTRIAL ELECTRONICS.